Semileptonic decays of heavy-flavour hadrons

Master's Thesis, 15.4.2023

Author:

ALEX TOLVANEN

Supervisors:

ILKKA HELENIUS
HANNU PAUKKUNEN

UNIVERSITY OF JYVÄSKYLÄ
DEPARTMENT OF PHYSICS

2

Abstract

Heavy-flavour hadrons, i.e. hadrons that contain at least one heavy quark, are interesting as their masses are large enough that it is possible to calculate their production cross sections even at small transverse momenta. As measuring the spectra for the hadrons themselves is not always possible, it is often useful to study the decay products, or more precisely their spectra. Semileptonic decay channels are particularly useful for this purpose since detecting decay particles, such as electrons and positrons, is often relatively easy.

In this thesis, we have developed a simulation that allows us to study the decay of heavy-flavour hadrons. The simulation uses production cross sections obtained using the so-called SACOT-m_T scheme as a starting point. Furthermore, the simulation uses the PYTHIA event generator to model the decay processes. In this work, the production cross sections of the decay particles, in this case electrons and positrons, are the main object of interest. Our aim is to assess the validity of the use of the SACOT-m_T scheme by comparing our numerical results with experimental results and FONLL calculations. We find that our numerical results are in good correspondence with experimental data and therefore we can consider our simulation to be successful. Thus, we can also conclude that the use of the SACOT-m_T scheme is justified in this context.

Keywords: heavy-flavour hadron, semileptonic decay, simulation, SACOT-m_T

Tiivistelmä

Tolvanen, Alex
Raskaiden hadronien semileptoniset hajoamiset
Pro gradu -tutkielma
Fysiikan laitos, Jyväskylän yliopisto, 2023, 55 sivua

Raskaat hadronit, eli hadronit jotka sisältävät vähintään yhden raskaan kvarkin, ovat kiinnostavia, koska niiden massat ovat tarpeeksi suuria jotta niiden tuottovaikutusalat voi laskea jopa pienillä poikittaisliikemäärillä. Koska itse hadronien spektrien mittaaminen ei ole aina mahdollista on usein hyödyllistä tutkia hajoamistuotteita, tai pikemminkin niiden spektrejä. Semileptoniset hajoamiskanavat ovat erityisen hyödyllisiä tähän tarkoitukseen sillä hajoamisessa syntyvien hiukkasten, tässä tapauksessa elektronien ja positronien, havaitseminen on yleensä suhteellisen helppoa.

Tässä tutkielmassa olemme kehittäneet simulaation, jonka avulla voidaan tutkia raskaiden hadronien hajoamisia. Tämä simulaatio käyttää niinkutsutun SACOT-m_{T} skeeman avulla saatuja tuottovaikutusaloja lähtökohtana. Lisäksi, simulaatio käyttää PYTHIA eventtigeneraattoria hajoamisprosessien mallintamiseen. Tässä työssä keskeisinä kiinnostuksen kohteina ovat hajoamistuotteiden tuottovaikutusalat. Tavoitteena on arvioida SACOT-m_{T} skeeman käytön pätevyyttä vertaamalla saatuja numeerisia tuloksia kokeellisiin tuloksiin ja FONLL laskuihin. Saatujen numeeristen tulosten havaitaan olevan hyvässä sopusoinnussa kokeellisen datan kanssa ja täten simulaatiota voidaan pitää onnistuneena. Näin ollen, voidaan myös todeta, että SACOT-m_{T} skeeman käyttäminen on tässä yhteydessä perusteltua.

Avainsanat: raskas hadroni, semileptoninen hajoaminen, simulaatio, SACOT-m_{T}

Preface

This thesis is the culmination of my time as a student here at the University of Jyväskylä. It has been a long and fulfilling process that has allowed me to familiarize myself with many topics and concepts I would most likely not have encountered otherwise. The numerical part of this thesis was done during my summer internship at the University of Jyväskylä, Department of Physics, and I am very grateful for this opportunity as it allowed me to focus on my thesis without interfering with my other studies.

I could not have done this without any help and thus I wish to express my gratitude to those who have aided me. First, I wish to thank my supervisors Ilkka Helenius and Hannu Paukkunen whose guidance and insight have been indispensable to me. Furthermore, I would like to thank Dong Jo Kim, who helped us obtain datapoints that had not yet been made publicly available at the time of writing, and Timothy Rinn, who was able to clarify some details about a recent paper from the PHENIX Collaboration, namely Phys.Rev.D 99 (2019) 9, 092003. Finally, I wish to thank my friends and family who have supported me throughout this process.

Jyväskylä April 15, 2023

Alex Tolvanen

Contents

1 Introduction

The year 1964 was groundbreaking for the field of particle physics. It was during this year that the existence of a type of sub-particles that made up the numerous known particles, considered at the time to be elementary particles, was first proposed. The existence of such particles was independently proposed by Murray Gell-Mann [1] and George Zweig [2]. These sub-particles have since become commonly known as quarks and they are the cornerstone of our understanding of the structure and behaviour of hadrons.

The original quark model that consisted of three quark flavours, namely up, down and strange, has since been supplemented with the existence of three other flavours, namely charm, bottom and top. The original three quark flavours are collectively referred to as light quarks whereas the other quark flavours are collectively referred to as heavy quarks. This distinction is due to the significant difference between the masses of light-flavour quarks, $m_u = 2.16$ MeV, $m_d = 4.67$ MeV and $m_s = 93.4$ MeV, and the heavy-flavour quarks, $m_c = 1.27$ GeV, $m_b = 4.18$ GeV and $m_t = 172.69$ GeV [3].

In this thesis, we focus on charm and bottom quarks, henceforth referred to as heavy quarks. More precisely, we are interested in heavy-flavour hadrons, by which we mean hadrons that contain at least one heavy quark. Henceforth, we will refer to hadrons containing at least one b quark as B-hadrons and we will similarly refer to hadrons containing at least one c quark as C-hadrons. Heavy quarks are particularly interesting, because their masses make it possible to calculate their production cross sections at low p_{T}, i.e. at low values of transverse momentum, using perturbative Quantum Chromodynamics (pQCD). Next-to-leading order calculations involve logarithms of the form $\log\left(\frac{p_{\mathrm{T}}}{m}\right)$ that become problematic if the mass is small. This property has given rise to the fixed-order-plus-next-to-leading-log (FONLL) approach [4], which has become an essential method of obtaining theoretical predictions and serves as reliable tool that can be used as a point of comparison for experimental data, as is done in Ref. [5]. Such experimental results have been obtained in the plethora of experimental studies that have been performed, for example at the Large

Hadron Collider (LHC) [6].

The experimental study of heavy-flavour hadrons is still being conducted and future research has been planned for example at A Large Ion Collider Experiment (ALICE) [7]. Therefore, since measuring the spectra of heavy-flavour hadrons is not always possible, it is imperative that we both understand and are able to model their decay processes and study the decay products. Due to the fact that heavy-flavour hadrons have significant semileptonic decay channels, one is able to study their properties through the observation of heavy-flavour electrons, by which we mean electrons produced in the decay process.

The goal of this work is to create a simulation program that models the decay of heavy-flavour hadrons and to obtain numerical estimates for the production cross sections of heavy-flavour electrons from both charm and bottom decays. Our aim is to compare the numerical estimates with theoretical predictions from FONLL calculations and experimental results obtained by the PHENIX Collaboration [5]. This will allow us to assess the validity of our approach and the underlying implementation of the general-mass variable-flavour-number scheme, the so-called SACOT-m_T scheme discussed in Ref. [8].

The structure of this thesis is as follows. In chapter 2 we shall discuss the theoretical background of this work. The discussion covers the most significant theoretical approaches to the production of heavy-flavour hadrons as well as the SACOT-m_T scheme. We will also discuss the decay processes of heavy-flavour hadrons and briefly explain how the PYTHIA event generator [9], models such decays. Chapter 3 will contain a detailed in-depth discussion of the numerical methods present in our simulation. In chapter 4 we present the numerical results and discuss the comparison between the numerical results, FONLL calculations and experimental results. Finally, in chapter 5 we present the final conclusions of this thesis.

In this thesis we shall use the common system of natural units in which the reduced Planck's constant and the speed of light are equated to unity: $\hbar = c = 1$.

2 Theoretical background

2.1 Parton-to-hadrons distribution functions

Parton distribution functions (PDFs) are essentially number densities for observing certain types of partons in a hadron. Let us assume that a parton of type a is found from a hadron of type A in such a way that it carries the fraction x of the hadron's momentum. The probability of observing such a parton, with $x \in [x, x + \mathrm{d}x]$, would then be [10]

$$P_a = f_a^A(x, \mu_{\text{fact}})\mathrm{d}x, \tag{2.1}$$

where $f_a^A(x, \mu_{\text{fact}})$ is the parton distribution function and μ_{fact} is the factorization scale. We note that the particle distribution functions themselves are obtained by performing a fit to experimental data in such a way that the experimental and theoretical cross sections agree with one another. For example, a fit to LHC data has been done in Ref. [11].

In order to understand the concept of factorization in this context, let us consider jet production of the form $A + B \to \text{Jet} + X$, where A and B are hadrons from which the partons a and b originate and a jet is essentially a well-collimated hadron shower that originates from the high-p_{T} quarks and gluons that are produced. Now, if $\frac{\mathrm{d}\hat{\sigma}}{\mathrm{d}P_{\text{T}}}$ is the differential cross section for partons a and b to produce the jet in question, the cross section for producing the jet is [10]

$$\frac{\mathrm{d}\sigma}{\mathrm{d}P_{\text{T}}} \sim \sum_{a,b} \int \mathrm{d}x_A f_a^A(x_A, \mu_{\text{fact}}) \int \mathrm{d}x_B f_b^B(x_B, \mu_{\text{fact}})\frac{\mathrm{d}\hat{\sigma}}{\mathrm{d}P_{\text{T}}}, \tag{2.2}$$

where the sum goes over the possible types of partons. In this case, the principle of factorization states that Eq. (2.2) must hold up to certain corrections. This includes corrections of order $\left(\frac{m}{P_{\text{T}}}\right)^n$, m being a typical hadronic mass scale and n being determined by the process

$$\frac{\mathrm{d}\hat{\sigma}}{\mathrm{d}P_{\text{T}}} \sim \sum_N \left(\frac{\alpha_s(\mu_{\text{ren}})}{\pi}\right)^N H_N(x_A, x_B, P_{\text{T}}; a, b; \mu_{\text{ren}}), \tag{2.3}$$

where μ_{ren} is the renormalization scale and the coefficients $H_N(x_A, x_B, P_{\mathrm{T}}; a, b; \mu_{\mathrm{ren}})$ are calculated using pQCD [10].

2.2 Parton fragmentation functions

As opposed to PDFs, which describe how partons are found in colour-neutral particles, parton fragmentation functions (FFs) describe how particles that have a colour charge, namely quarks and gluons, transform into colour-neutral final-state particles such as hadrons. More precisely, parton fragmentation functions are probability densities for producing colour-neutral particles from partons [12].

In this thesis, we have used the well-known unpolarized fragmentation function $D^{h/i}(z)$. The fragmentation function $D^{h/i}(z)$ describes how an unpolarized parton of type i fragments into an unpolarized hadron of type h in such a way that the hadron carries the fraction z of the parton's momentum [12]. As such, we obtain the number of hadrons of type h, with $z \in [z, z + \mathrm{d}z]$, observed in a parton of type i as

$$N_h = D^{h/i}(z)\mathrm{d}z. \tag{2.4}$$

The importance of the concept of FFs, as well as PDFs, becomes apparent when considering the cross section of single-inclusive hadron production in, for example, a proton-proton collision, $p + p \rightarrow h + X$. Now in order to calculate the cross section for such a process we would need to know the relevant fragmentation function and parton distribution functions and also the partonic cross section, $\hat{\sigma}$, for the process in question.

2.3 Hadroproduction

In this section, we shall briefly present some of the most significant theoretical approaches to heavy-flavour production. Our discussion will include the fixed-flavour-number scheme (FFNS), the zero-mass variable flavour number scheme (ZM-VFNS), the general-mass variable flavour number scheme (GM-VFNS) and the fixed-order-plus-next-to-leading-log (FONLL) approach, which is one of the most significant GM-VFNS approaches. We shall, however, limit our discussion to heavy-flavour production in proton-proton collisions.

2.3.1 FFNS

The fixed-flavour-number scheme can be considered the simplest approach to open-heavy-flavour production. This is due to the fact that the heavy quark is not treated as an active parton in the proton. In this framework, the differential cross section for the inclusive production of a heavy quark, denoted as Q, is obtained as [6]

$$\mathrm{d}\sigma^{Q+X}[s, p_{\mathrm{T}}, y, m_Q] \simeq \sum_{i,j} \int_0^1 \mathrm{d}x_i \int_0^1 \mathrm{d}x_j f_i^A(x_i, \mu_{\mathrm{fact}}) f_j^B(x_j, \mu_{\mathrm{fact}}) \mathrm{d}\tilde{\sigma}_{ij \to Q+X}[x_i, x_j,$$

$$s, p_{\mathrm{T}}, y, m_Q, \mu_{\mathrm{fact}}, \mu_{\mathrm{ren}}]. \tag{2.5}$$

In equation (2.5) s is the squared hadron center-of-mass energy, m_Q is the mass of the heavy quark, f_i^A and f_j^B are the parton distribution functions and μ_{fact} and μ_{ren} are the factorisation and renormalization scales respectively. Finally, $\mathrm{d}\tilde{\sigma}$ is the partonic cross section from which the collinear singularities associated with the gluon and the light quarks have been removed.

Equation (2.5) contains a sum over all possible subprocesses $i + j \to Q + X$, where i and j are the active partons in the proton. We may then use one of two approaches: FFNS with three active flavours, $i, j \in \{q, \bar{q} = (u, \bar{u}, d, \bar{d}, s, \bar{s}), g\}$, or FFNS with four active flavours, $i, j \in \{q, \bar{q} = (u, \bar{u}, d, \bar{d}, s, \bar{s}, c, \bar{c}), g\}$, where the charm quark is treated as an active parton for $\mu_{\mathrm{fact}} > m_c$ and where we neglect m_c in $\mathrm{d}\tilde{\sigma}$ [6]. The fixed-flavour-number scheme with three flavours can be used for both charm and bottom production, whereas FFNS with four flavours can only be used for bottom production.

We know that at the leading order in α_s, the strong coupling constant, there are only two contributing sub-processes, namely $q + \bar{q} \to Q + \bar{Q}$ and $g + g \to Q + \bar{Q}$. Furthermore, we must, at the next-to-leading order, include the virtual one-loop corrections to the aforementioned sub-processes as well as the following sub-processes [6]:

$$q + \bar{q} \to Q + \bar{Q} + g,$$
$$g + g \to Q + \bar{Q} + g,$$
$$g + q \to q + Q + \bar{Q},$$
$$g + \bar{q} \to \bar{q} + Q + \bar{Q}.$$

Complete next-to-leading order calculations for the cross section for heavy-flavour

production have been performed, for example, in Ref. [13] and Ref. [14]. Finally, we note that at the next-to-leading order the FFNS is applicable approximately within the range $0 \leq p_{\mathrm{T}} \lesssim 5 \times m_Q$ beyond which the FFNS prediction begins to overestimate the cross section [6].

2.3.2 ZM-VFNS

The logarithms involving the heavy-quark mass, $\frac{\alpha_s}{2\pi}\ln(\frac{p_{\mathrm{T}}^2}{m_Q^2})$, which are present in the partonic cross section $\mathrm{d}\tilde{\sigma}$, clearly become large in the region $p_{\mathrm{T}} \gg m_Q$. Therefore, the logarithms must eventually be resummed to all orders in the perturbation theory, which is done by absorbing them into the PDFs and FFs. As a result, the FFs become scale-dependent. In this approach the heavy-quark must be treated as an active parton for factorization scales $\mu_{\mathrm{fact}} \geq \mu_{\mathrm{tran}}$ where the transition scale, μ_{tran}, is generally identified with the heavy-quark mass [6]. Thus, we have a scheme in which the number of active flavours changes when the transition scale is crossed. This is known as a variable flavour number scheme.

The zero-mass variable flavour number scheme is a special case of the variable flavour-number scheme in which we neglect the heavy-quark mass when calculating the short-distance cross section, $\mathrm{d}\hat{\sigma}_{ij \to k+X}$. Because of this, the ZM-VFNS only produces accurate predictions for the region of large transverse momentum. In the ZM-VFNS the differential cross section for producing a heavy-flavour hadron, in a process of the form $A + B \to H + X$ is obtained from the following equation [6]

$$\mathrm{d}\sigma^{H+X} \simeq \sum_{i,j,k} \int_0^1 \mathrm{d}x_i \int_0^1 \mathrm{d}x_j \int_0^1 \mathrm{d}z f_i^A(x_i, \mu_{\mathrm{fact}}) f_j^B(x_j, \mu_{\mathrm{fact}}) \mathrm{d}\hat{\sigma}_{ij \to k+X}$$

$$D_k^H(z, \mu_{\mathrm{fact}}') + \mathcal{O}\left(\frac{m_Q^2}{p_{\mathrm{T}}^2}\right). \tag{2.6}$$

A complete NLO calculation of all sub-processes has already been performed, for example, in Ref. [15].

2.3.3 GM-VFNS

Both the FFNS and the ZM-VFNS are good methods for calculating the cross section for heavy-flavour production but they are only valid in limited p_T regions. The general-mass variable flavour number scheme combines the benefits of the fixed-order (FO) calculations in the FFNS at low p_T and the massless calculation in the ZM-VFNS at high p_T in order to generate a framework that is valid over the entire kinematic range. To be precise, the large logarithms are resummed by the Dokshitzer-Gribov-Lipatov-Altarelli-Parisi (DGLAP) evolution [16–19] of nonperturbative fragmentation functions and PDFs and the mass-dependent terms from the FFNS are retained [20]. The differential cross section for the production of heavy-flavour hadrons is obtained from [6]

$$
\mathrm{d}\sigma^{H+X} \simeq \sum_{i,j,k} \int_0^1 \mathrm{d}x_i \int_0^1 \mathrm{d}x_j \int_0^1 \mathrm{d}z f_i^A(x_i, \mu_\mathrm{fact}) f_j^B(x_j, \mu_\mathrm{fact}) \mathrm{d}\hat{\sigma}_{ij \to k+X}[p_\mathrm{T}, m_Q]
$$
$$
D_k^H(z, \mu'_\mathrm{fact}). \tag{2.7}
$$

Next-to-leading order calculations for the cross section of heavy-flavour production in proton-proton collisions have been discussed for example in Ref. [20] and Ref. [21].

The GM-VFNS succesfully combines the benefits of the FFNS and the ZM-VFNS but the use of the zero-mass approximation can lead to some problems. To be precise, these problems occur in some applications of the GM-VFNS when the fragmenting parton is a light one or when there are heavy-quarks in the initial state of the process [8]. At large p_T, more precisely when $p_\mathrm{T} \gg m_Q$, the results of the GM-VFNS approach the results of the ZM-VFNS as we would expect. However, at low p_T the massless coefficient functions display divergent behaviour which causes the cross sections to diverge as p_T approaches zero. This behaviour makes obtaining a well-behaved description for the heavy-flavour hadrons, that is valid through the entire kinematic range, rather difficult. These significant issues have motivated the need for general-mass variable flavour number schemes that circumvent them. One such scheme is the SACOT-m_T scheme which is discussed in section 2.4.

2.3.4 FONLL

One of the most significant general-mass variable flavour number schemes is the FONLL approach. The FONLL approach is a particularly significant theoretical framework in the study of heavy-flavour production that is valid through the entire kinematic range. As the FONLL approach is a general-mass variable flavour number scheme, it combines the virtues of the FFNS and the ZM-VFNS. The main idea is linked to how the leading-logarithmic terms (LL), $\alpha_s^2(\alpha_s\log\frac{p_\mathrm{T}}{m})^k$, and next-to-leading logarithmic terms (NLL), $\alpha_s^3(\alpha_s\log\frac{p_\mathrm{T}}{m})^k$, that arise in the power expansion of the cross section, are treated.

To be precise, the FONLL approach combines two different approaches to handling these terms, namely an order-α_s^3 calculation, referred to as the fixed-order approach, and another calculation, referred to as the resummed-approach (RS), where the LL and NLL corrections are calculated with the fragmentation function formalism [22]. Furthermore, all terms of order α_s^2, α_s^3, $\alpha_s^2\alpha_s^k\log^k\left(\frac{p_\mathrm{T}}{m}\right)$ and $\alpha_s^3\alpha_s^k\log^k\left(\frac{p_\mathrm{T}}{m}\right)$ are included exactly.

The cross section is obtained by combining the result of the FO calculation at NLO [4]

$$\frac{\mathrm{d}\sigma}{\mathrm{d}p_\mathrm{T}^2} = A(m)\alpha_s^2 + B(m)\alpha_s^3 + \mathcal{O}(\alpha_s^4), \tag{2.8}$$

and the RS calculation at NLL [4]

$$\frac{\mathrm{d}\sigma}{\mathrm{d}p_\mathrm{T}^2} = \alpha_s^2 \sum_{i=0}^{\infty} a_i \left(\alpha_s\log\frac{\mu}{m}\right)^i + \alpha_s^3 \sum_{i=0}^{\infty} b_i \left(\alpha_s\log\frac{\mu}{m}\right)^i$$
$$+ \mathcal{O}\left(\alpha_s^4\left(\alpha_s\log\frac{\mu}{m}\right)^i\right) + \mathcal{O}(\alpha_s^2 \times \mathrm{PST}), \tag{2.9}$$

where a_i and b_i are coefficients that depend on the center-of-mass energy E_cm, p_T and μ. In equation (2.9) PST refers to the terms that are suppressed by the powers of $\frac{m}{p_\mathrm{T}}$, and thus neglected. In the FONLL approach the equations (2.8) and (2.9) are combined in such a way that we obtain

$$\frac{\mathrm{d}\sigma}{\mathrm{d}p_\mathrm{T}^2} = A(m)\alpha_s^2 + B(m)\alpha_s^3 + \left(\alpha_s^2 \sum_{i=2}^{\infty} a_i \left(\alpha_s\log\frac{\mu}{m}\right)^i + \alpha_s^3 \sum_{i=1}^{\infty} b_i \left(\alpha_s\log\frac{\mu}{m}\right)^i\right)$$
$$\times G(m, p_\mathrm{T}) + \mathcal{O}\left(\alpha_s^4\left(\alpha_s\log\frac{\mu}{m}\right)^i\right) + \mathcal{O}(\alpha_s^4 \times \mathrm{PST}), \tag{2.10}$$

where $G(m, p_T)$ is some arbitrary function that approaches 1 when $\frac{m}{p_\mathrm{T}} \to 0$ [4]. The function $G(m, p_T)$ appears due to the fact that $G(m, p_T) = 1 + \mathrm{PST}$, and thus Eq. (2.9) can be written in the form

$$\frac{\mathrm{d}\sigma}{\mathrm{d}p_\mathrm{T}^2} = G(m, p_T)\left(\alpha_s^2 \sum_{i=0}^{\infty} a_i \left(\alpha_s \log\frac{\mu}{m}\right)^i + \alpha_s^3 \sum_{i=0}^{\infty} b_i \left(\alpha_s \log\frac{\mu}{m}\right)^i\right)$$
$$+ \mathcal{O}\left(\alpha_s^4 \left(\alpha_s \log\frac{\mu}{m}\right)^i\right) + \mathcal{O}(\alpha_s^2 \times \mathrm{PST}). \tag{2.11}$$

In order to complete the calculation we need an approximation of the FO calculation at the so-called massless limit (FOM0), where the finite power-like mass terms may be neglected. This is due to the fact that we need to subtract the fixed-order terms, that are already present in the FO result, from the RS result. The FOM0 cross section is

$$\frac{\mathrm{d}\sigma}{\mathrm{d}p_T^2} = a_0\alpha_s^2 + \left(a_1 \log\frac{\mu}{m} + b_0\right)\alpha_s^3 + \mathcal{O}(\alpha_s^2 \times \mathrm{PST}), \tag{2.12}$$

which is obtained from equation (2.8) by using the following properties $A(m) = a_0 + \mathrm{PST}$ and $B(m) = a_1 \log\frac{\mu}{m} + b_0 + \mathrm{PST}$ [4]. Now we obtain the FONLL cross section as [6]

$$\mathrm{d}\sigma_\mathrm{FONLL} = \mathrm{d}\sigma_\mathrm{FO} + G(m_Q, p_\mathrm{T}) \times (\mathrm{d}\sigma_\mathrm{RS} - \mathrm{d}\sigma_\mathrm{FOM0}), \tag{2.13}$$

where $G(m_Q, p_\mathrm{T})$ is a matching function that ensures that the conditions $\mathrm{d}\sigma_\mathrm{FONLL} \to \mathrm{d}\sigma_\mathrm{RS}$ for $p_\mathrm{T} \gg m_Q$ and $\mathrm{d}\sigma_\mathrm{FONLL} \to \mathrm{d}\sigma_\mathrm{FO}$ for $p_\mathrm{T} \to 0$ are fulfilled. In the FONLL approach the function $G(m_Q, p_\mathrm{T})$ is chosen to be [6]

$$G(m_Q, p_\mathrm{T}) = \frac{p_\mathrm{T}^2}{p_\mathrm{T}^2 + a^2 m_Q^2}, \tag{2.14}$$

where one chooses $a = 5$.

2.4   SACOT-m_T scheme

2.4.1   Background

As mentioned in section 2.3.3, the difficulties in obtaining a well-behaved description for the heavy-flavour hadrons, that is valid through the entire kinematic range, in the GM-VFNS have motivated the need for other general-mass variable flavour number schemes that circumvent these issues. The SACOT-m_T scheme, first suggested in Ref. [8], is one such scheme. It takes advantage of the scheme dependence present in the GM-VFNS in order to prevent the problematic divergent behaviour at low p_T with a convenient choice of scheme.

The choice of scheme is based on the observation that, in the absence of intrinsic charm components, the contributions from both the heavy-quark PDFs and the light parton FFs can be regarded as an efficient way to resum diagrams where a heavy quark-antiquark pair is dynamically produced [8]. These contributions can then be required to obey the same kinematic constraints as the channels where the pair is explicitly produced. Including these effects in the definition of the scheme will then lead to the contributions from the heavy-quark PDFs and light parton FFs that are regulated by the heavy-quark mass, thus preventing the divergent behaviour in the production cross sections when $p_\mathrm{T} \to 0$.

2.4.2   Kinematics

The SACOT-m_T scheme was developed for the study of inclusive hadroproduction of heavy-flavour hadrons. Specifically the process

$$h_1(P_1) + h_2(P_2) \to h_3(P_3) + X,$$

where h_1, h_2 and h_3 refer to hadrons and P_1, P_2 and P_3 to their respective momenta. This process is illustrated in Figure 1. If the masses of partons and the produced

hadron are neglected, the differential cross section has the factorized form

$$\frac{\mathrm{d}\sigma(h_1 + h_2 \to h_3 + X)}{\mathrm{d}P_\mathrm{T}\mathrm{d}Y} = \sum_{ijk} \int_{z^{\min}}^1 \frac{\mathrm{d}z}{z} \int_{x_1^{\min}}^1 \mathrm{d}x_1 \int_{x_2^{\min}}^1 \mathrm{d}x_2$$

$$D_{k \to h_3}(z, \mu_\mathrm{frag}^2) f_i^{h_1}(x_1, \mu_\mathrm{fact}^2) f_j^{h_2}(x_2, \mu_\mathrm{fact}^2)$$

$$\frac{\mathrm{d}\hat{\sigma}^{ij \to k}(\tau_1, \tau_2, \mu_\mathrm{ren}^2, \mu_\mathrm{fact}^2, \mu_\mathrm{frag}^2)}{\mathrm{d}p_\mathrm{T}\mathrm{d}y}, \tag{2.15}$$

where P_T and Y refer to the hadron's transverse momentum and rapidity whereas p_T and y refer to the fragmenting parton's transverse momentum and rapidity [8]. In equation (2.15), $f_i^{h_1}(x_1, \mu_\mathrm{fact}^2)$ and $f_j^{h_2}(x_2, \mu_\mathrm{fact}^2)$ are the PDFs for parton species i and j in hadrons h_1 and h_2 respectively and $D_{l \to h_3}(z, \mu_\mathrm{frag}^2)$ is the parton-to-hadron, specifically h_3, FF. Furthermore, the invariants are defined as [8]

$$\tau_1 \equiv \frac{p_1 \cdot p_3}{p_1 \cdot p_2} = \frac{p_\mathrm{T}e^{-y}}{x_2\sqrt{s}}, \quad \tau_2 \equiv \frac{p_2 \cdot p_3}{p_1 \cdot p_2} = \frac{p_\mathrm{T}e^{y}}{x_1\sqrt{s}}, \tag{2.16}$$

where p_1, p_2 and p_3 are the momenta of the partons, p_1 and p_2 refer to the incoming partons and p_3 to the produced parton, and $\sqrt{s}$ is the center-of-mass energy of the process. Finally, the integration limits arising from kinematic constraints in
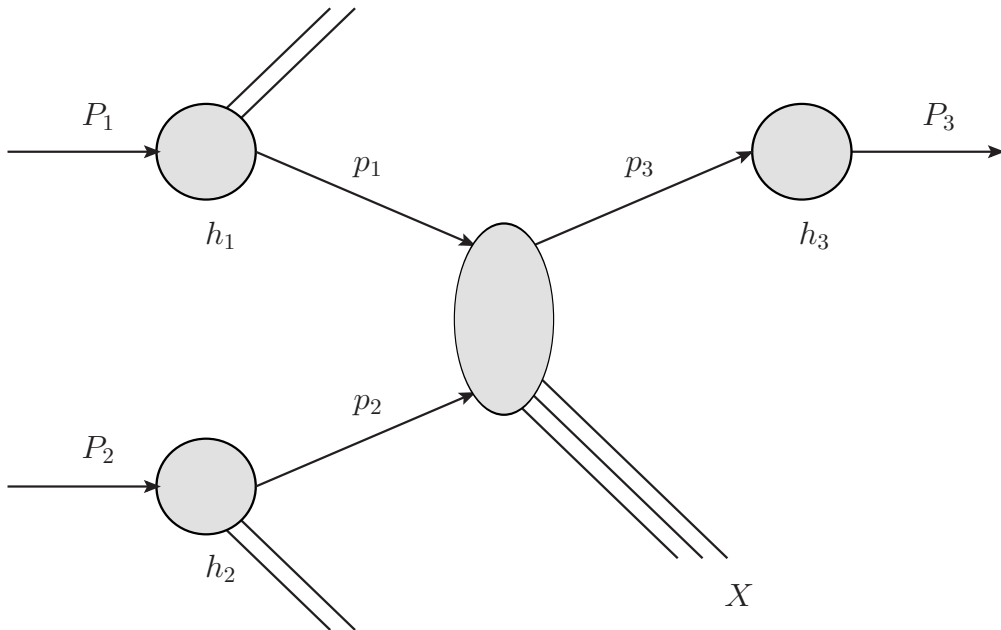

Figure 1. Illustration of the process $h_1(P_1) + h_2(P_2) \to h_3(P_3) + X$.

equation (2.15) are [8]

$$x_1^{\text{min}} = \frac{p_{\text{T}} e^y}{\sqrt{s} - p_{\text{T}} e^{-y}}, \quad x_2^{\text{min}} = \frac{x_1 p_{\text{T}} e^{-y}}{x_1 \sqrt{s} - p_{\text{T}} e^y}, \quad z^{\text{min}} = \frac{2 P_{\text{T}} \cosh Y}{\sqrt{s}}. \tag{2.17}$$

Since we are dealing with heavy-flavour production the zero-mass partonic kinematics need to be adjusted so that the heavy-quark mass, m_Q, is taken into account. This is essentially done by replacing the transverse momentum p_{T} in the expressions for τ_1, τ_2, x_1^{min} and x_2^{min}, equations (2.16) and (2.17), with the transverse mass $m_{\text{T}} = \sqrt{p_{\text{T}}^2 + m_Q^2}$. Furthermore, since we cannot use the zero-mass version of the fragmentation scaling variable z, we define it in a Lorentz invariant manner

$$z \equiv \frac{P_3 \cdot (P_1 + P_2)}{p_3 \cdot (P_1 + P_2)}, \tag{2.18}$$

which obeys $z \to \frac{E_{\text{hadron}}}{E_{\text{parton}}}$ in the hadronic center-of-mass frame. If we assume that the collision is collinear in the center-of-mass frame and use equation (2.18), we obtain the following equations

$$z = \frac{M_{\text{T}} \cosh(Y)}{m_{\text{T}} \cosh(y)}, \tag{2.19}$$

$$\frac{P_{\text{T}}}{M_{\text{T}} \sinh(Y)} = \frac{p_{\text{T}}}{m_{\text{T}} \sinh(y)}, \tag{2.20}$$

where M is the mass of the produced hadron and $M_{\text{T}} = \sqrt{M^2 + P_{\text{T}}^2}$ is its transverse mass [8]. The equations (2.19) and (2.20) can then be solved in order to obtain expressions for the hadronic transverse momentum and rapidity, namely

$$P_{\text{T}}^2(y, p_{\text{T}}) = \frac{z^2 m_{\text{T}}^2 \cosh^2(y) - M^2}{1 + (m_{\text{T}}^2 \sinh^2(y))/p_{\text{T}}^2}, \tag{2.21}$$

$$Y(y, p_{\text{T}}) = \sinh^{-1} \left(\frac{m_{\text{T}} \sinh(y)}{p_{\text{T}}} \frac{P_{\text{T}}}{M_{\text{T}}} \right). \tag{2.22}$$

Finally the expression for the cross section that corresponds to our definition of the

scaling variable is [8]

$$\frac{\mathrm{d}\sigma(h_1 + h_2 \to h_3 + X)}{\mathrm{d}P_\mathrm{T}\mathrm{d}Y} = \sum_{ijk} \int_{z^\mathrm{min}}^1 \mathrm{d}z \int_{x_1^\mathrm{min}}^1 \mathrm{d}x_1 \int_{x_2^\mathrm{min}}^1 \mathrm{d}x_2 \int \mathrm{d}y \int \mathrm{d}p_\mathrm{T}$$
$$D_{k \to h_3}(z, \mu_\mathrm{frag}^2) f_i^{h_1}(x_1, \mu_\mathrm{fact}^2) f_j^{h_2}(x_2, \mu_\mathrm{fact}^2)$$
$$\frac{\mathrm{d}\hat{\sigma}^{ij \to k}(\tau_1, \tau_2, m_Q, \mu_\mathrm{ren}^2, \mu_\mathrm{fact}^2, \mu_\mathrm{frag}^2)}{\mathrm{d}p_\mathrm{T}\mathrm{d}y}$$
$$\delta(Y - Y(y, p_\mathrm{T}))\delta(P_\mathrm{T} - P_\mathrm{T}(y, p_\mathrm{T})). \tag{2.23}$$

Now, if we use the relation $\int \mathrm{d}y\mathrm{d}p_\mathrm{T} = \frac{1}{z}\int \mathrm{d}P_\mathrm{T}(y, p_\mathrm{T})\mathrm{d}Y(y, p_\mathrm{T})$, equation (2.23) becomes identical to equation (2.15), with the distinction that

$$p_\mathrm{T}^2 = \frac{M_\mathrm{T}^2\cosh^2(Y) - z^2 m_Q^2}{z^2}\left(1 + \frac{M_\mathrm{T}^2\sinh^2(Y)}{P_\mathrm{T}^2}\right)^{-1}, \tag{2.24}$$

$$y = \sinh^{-1}\left(\frac{M_\mathrm{T}\sinh(Y)}{P_\mathrm{T}}\frac{p_\mathrm{T}}{m_\mathrm{T}}\right), \tag{2.25}$$

$$z^\mathrm{min} = \frac{2M_\mathrm{T}\cosh(Y)}{\sqrt{s}}. \tag{2.26}$$

We note that in our implementation we use the following definition for the fragmentation scaling variable z instead of the one given in Eq. (2.18)

$$z \equiv \frac{P_3 \cdot (P_1 - P_2)}{p_3 \cdot (P_1 - P_2)}. \tag{2.27}$$

The reason for this is that using the definition of z given in Eq. (2.18) leads to problematic behaviour for the double differential cross section around rapidity $y = 0.00$ at low p_T. This is due to the fact that if the definition given in Eq. (2.18) is used, heavy quarks will not form heavy-flavour mesons at sufficiently low p_T, as discussed in Ref. [23].

2.4.3   Partonic cross section

In order to obtain partonic cross sections in the SACOT-m_T scheme, we must first consider NLO one-particle inclusive heavy-quark cross section in the FFNS. In this case, heavy quark production, where a $q\bar{q}$ pair is produced, only occurs in the following partonic processes:

$$q + \bar{q} \to Q + \bar{Q} + X,$$
$$q + g \to Q + \bar{Q} + X,$$
$$g + g \to Q + \bar{Q} + X.$$

In the ZM-VFNS calculation, the partonic cross sections then develop logarithmic divergences in the high-p_T limit. These logarithmic divergences come from the kinematic regions where the quarks become collinear with other partons [8]. As discussed in the section 2.3.3 these logarithms are resummed when the interaction scale exceeds the chosen transition scale which in the SACOT-m_T scheme is identified as the heavy-quark mass, $\mu_T = m_Q$.

If left unaddressed, taking the contributions from both the heavy-quark PDFs and parton-to-hadron FFs into account would lead to double counting. In order to avoid this, the logarithmic terms must be subtracted from the coefficient functions. To be precise, this is done by determining the correct subtraction terms which, at NLO, can be done by considering the LO contributions from the channels where the fragmenting parton is light or where the initial state contains heavy-quarks. These contributions uniquely determine the correct subtraction terms, which can then be taken into account.

This reasoning can now be applied to the aforementioned partonic processes. A detailed discussion of how this is done in practice has been given in Ref. [8] and therefore we shall not go into detail here. However, we mention that the exact form of the multiplied matrix element can be chosen at will as long as it tends to its zero-mass expression at the $m \to 0$ limit. This is important because the integration limits mentioned in the previous section behave similarly. Therefore, we may choose the simplest possibility, namely using the zero-mass matrix element and kinematics discussed in section 2.4.2, which is usually called the simplified ACOT, SACOT, scheme. Finally, we note that the SACOT-m_T scheme takes into account the $\mathcal{O}(\alpha_s^3)$ contributions from Ref. [15] and the contributions from all other partonic

subprocesses whose inclusion does not require the subtraction of terms at NLO [8].

2.5   Decay processes

As mentioned in section 1, heavy-flavour hadrons have significant semileptonic decay channels. For example, the B^- meson has the decay channel $B^- \rightarrow e^- \bar{\nu}_e X_c$, where X_c refers to any C-hadron, with a branching fraction of $(10.8 \pm 0.4)\%$ and the D^+ meson has the decay channel $D^+ \rightarrow \bar{K}^0 e^+ \nu_e$ with a branching fraction of $(8.72 \pm 0.09)\%$ [3]. Heavy-flavour decays are largely defined by the decay processes of the heavy-quarks. Therefore, it is imperative to understand how a heavy quark can transform into a lighter quark by emitting a $W^\pm$ boson. This is essentially what happens when a heavy-flavour hadron decays through a semileptonic decay channel.

Let us consider the B^- decay $B^- \rightarrow e^- \bar{\nu}_e D^0$ in the lowest order. Here the b quark transforms into a lighter quark, namely the c quark, through the weak interaction. This involves emitting a W^- boson, which then decays into an electron and an electron antineutrino. If we consider the D^+ decay $D^+ \rightarrow e^+ \nu_e \bar{K}^0$ in the lowest order, we again find that the heavy quark decays into a lighter one through the weak interaction. In this case, the c quark transforms into a s quark by emitting a W^+ boson, which decays into a positrons and an electron neutrino. The Feynman diagrams of these decays are displayed in Figures 2 and 3 respectively.

As one might imagine, these simple decay processes become much more difficult as higher-order contributions are taken into account. However, the weak interaction still plays a central part in all contributions. We omit a detailed discussion of the higher order contributions as it would be beyond the scope of this thesis. Furthermore, as we have used the PYTHIA event generator to model the decay events, we must discuss how PYTHIA models these decays. The following section is dedicated to briefly discussing heavy-flavour decays from the perspective of the PYTHIA event generator.
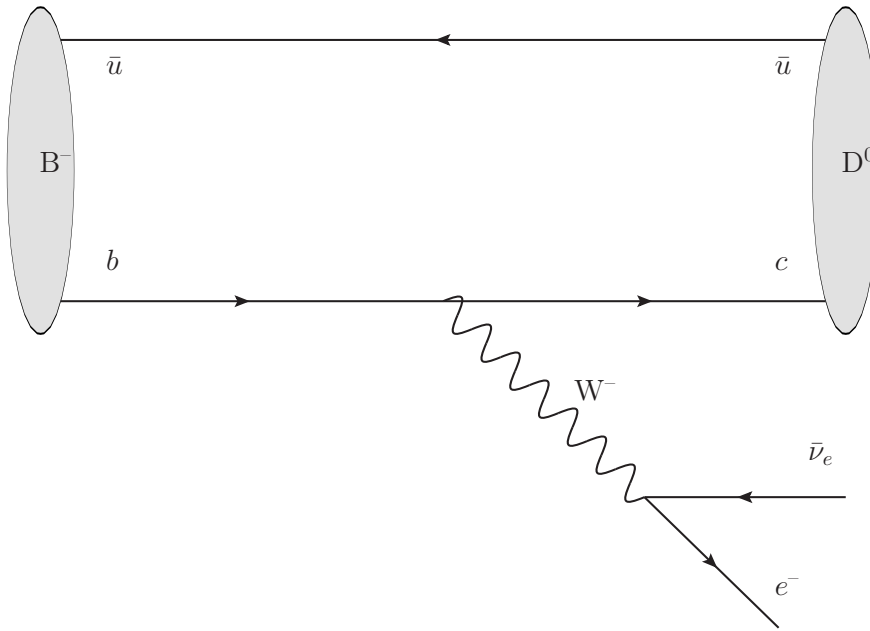
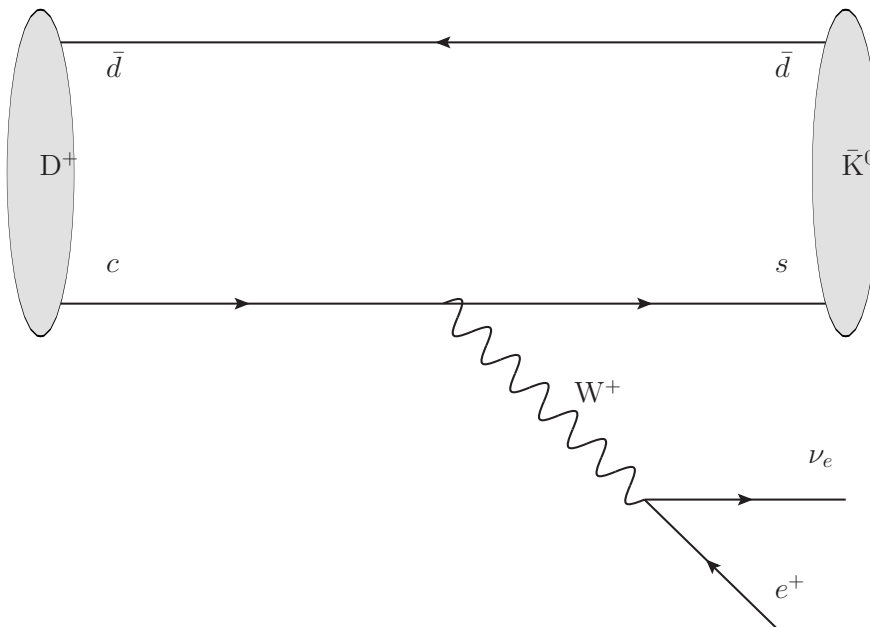**Figure 2.** Feynman diagram for the decay $B^- \to e^- \bar{\nu}_e D^0$.

Figure 3. Feynman diagram for the decay $D^+ \to e^+ \nu_e \bar{K}^0$.

2.6 Weak decays in PYTHIA

In order to properly understand how heavy-flavour decays are numerically modelled we will briefly discuss how heavy-flavour decays are processed in PYTHIA 8.3. Knowledge about the properties, such as mass or decay channels, of different particles are a built-in part of the PYTHIA 8.3 framework. PYTHIA applies measured branching ratios to sample the decay channel and decay products. In fact, in PYTHIA 8.3 the decay channels of all the hadrons whose decays we wish to model are based on the LHCb decay tables.

Once all relevant properties have been specified, the decay channel are randomly chosen from a list of possible decay channels with weights proportional to their respective branching fractions [9]. The decay products must also be distributed according to the phase space. This is not necessarily trivial and therefore in PYTHIA 8.3 this is done using specialized algorithms that are presented in Ref. [9]. We will henceforth limit our discussion to the decay events for which PYTHIA 8.3 has dedicated matrix elements.

In this work, we are interested in semileptonic decays that always occur through the weak interaction. In what follows, we will discuss how weak decays are handled in PYTHIA, using the semileptonic decay channel $B^- \rightarrow e^- \bar{\nu}_e D^0$, which is discussed above and illustrated in Figure 2, as an example. The idea is to use the unpolarized matrix element for the t-channel weak scattering of fermions, $f_0 f_1 \rightarrow f_2 f_3$,

$$|\mathcal{M}|^2 \propto (p_0 p_1)(p_2 p_{\mathrm{rem}}), \tag{2.28}$$

where p_i is the momentum of the fermion f_i and p_{rem} is the sum of the remaining momenta, which in this case is merely p_3, to approximate the semileptonic decays of heavy-flavour hadrons [9]. By using crossing symmetry, this matrix element can be used for the decay process $f_0 \rightarrow f_1 f_2 f_3$. One example of such a decay is the muon decay which is discussed for example in Ref. [24].

In PYTHIA, the idea is to ignore the light quarks and treat the decaying hadron as if it was only composed of the heavy quark. In essence, PYTHIA models the decay of the heavy quark and takes the light quarks into account when determining the decay products. The semileptonic decays can then be specified with their partonic content. Finally, the parton system is collapsed into a hadron according to the flavour-selection rules present in PYTHIA [9].

3   Numerical methods

The main purpose of this work was to numerically model the decay of heavy-flavour hadrons. To this end, we have constructed a simulation that takes a heavy-flavour hadron with arbitrary values of transverse momentum and rapidity, uses the PYTHIA event generator to model its decay process and processes the results.

In this section, we shall describe in detail the structure and implementation of this simulation. We will also present the performed normalizations and explain the chosen method for estimating the uncertainty associated with the results. For the sake of reproducibility, the entire simulation code alongside its command and header files and all separate scripts used for plotting have been made available as mentioned in Appendix A.

3.1   Initialization

Before the simulation can begin, we need to specify what we specifically wish to study. First, we must specify the data we wish to use. In this work, we use the data obtained with the numerical implementation of the SACOT-m_T scheme, discussed in Ref. [8], as a starting point.

Using this numerical implementation, we have obtained values for the double differential production cross section, $\frac{\mathrm{d}^2\sigma}{\mathrm{d}P_\mathrm{T}\mathrm{d}Y}$, for B$^+$ and D^0 mesons at certain values of transverse momentum and rapidity, N.B. the transverse momentum and rapidity are studied within the intervals 0.0 GeV $\leq P_\mathrm{T} \leq 20.0$ GeV and $-2.0 \leq Y \leq 2.0$. Using the numerical implementation of the SACOT-m_T scheme we have obtained datapoints within these intervals in such a manner that the values of p_T are 0.5 GeV apart and the values of rapidity are 0.25 apart.

More precisely, we have obtained sets of such values with the different possible variations of the factorization, renormalization and fragmentation scales, $(\mu_\mathrm{fact}, \mu_\mathrm{ren}, \mu_\mathrm{frag})$. We have then used these values to create tables from which we can then interpolate the cross section at arbitrary values of transverse momentum and rapidity, within

the studied intervals. These tables have been collected into external files and thus we must specify the desired one at the start of the simulation.

When starting the simulation both the decaying particles and the type of decay particles which we wish to study must be specified. We note that currently we have only studied the electrons/positrons that are formed in the decays. However, the framework could also be used to study other types of decay particles. Finally, we specify a set of seeds for random number generation.

Once the necessary settings have been specified, the data obtained using the numerical implementation of the SACOT-m_{T} scheme is read from an external file. After the data have been read, we define the necessary variables and histograms and specify the individual bins in the histograms. In this work, we have defined the bins of the histograms to be identical to those used in Ref. [5] so that we will be able to compare our results to the experimental results of the PHENIX Collaboration. Finally, once all this has been done we initialize the PYTHIA event generator in order to begin the event generation loop.

3.2   Decay event generation and processing

The event generation loop begins with the precise specification of the decaying particle. This is done by checking whether we are studying B- or C-hadrons, and by determining a specific hadron according to branching fractions. To be precise, we specify the PDG particle code that is used to identify the particle in PYTHIA 8.3 [9]. The possible decaying particles and their fragmentation fractions are known for B-hadrons from Ref. [3] and for C-hadrons from Ref. [25]. These fractions are listed in Tables 1 and 2.

Table 1. B-hadron fragmentation fractions from Ref.[3].

B-hadron	Production fraction
B^+	$(40.8 \pm 0.7)\%$
B^0	$(40.8 \pm 0.7)\%$
B^0_s	$(10.0 \pm 0.8)\%$
b-baryon	$(8.4 \pm 1.1)\%$

Table 2. C-hadron fragmentation fractions from Ref.[25].

C-hadron	Production fraction
D^+	0.232 ± 0.010
D^0	0.573 ± 0.023
D_s	0.080 ± 0.006
Λ_c	0.104 ± 0.010

Once the decaying particle has been specified we also need to define its four-momentum. This is done by first using PYTHIA to find the mass, m, of the decaying particle and then randomly sampling values for transverse momentum and rapidity, within the studied intervals, and for the azimuthal angle θ. We note that the values of P_T and rapidity are sampled from a flat probability distribution. This approach was chosen because it made it possible to obtain good statistics throughout the entire kinematic range. Furthermore, as we use the double differential cross sections as weights for the events, we are able to compensate for not sampling the kinematics according to the cross section. Thus, there was no explicit need to sample the values of P_T and rapidity from realistic distributions.

The sampled values of P_T and rapidity are also used to interpolate the corresponding cross section from the input data. This value is only valid for a certain meson, in this case either B^+ or D^0, and must therefore be scaled to account for other possible B- or C-hadrons. The scaling factor is obtained as the inverse of the production fraction of the meson the table was originally generated for. These fractions for B^+ and D^0 are listed in Tables 1 and 2. The hadron's four-momentum, $P = (E, P_x, P_y, P_z)$, can then be specified with the known equations

$$m_\text{T} = \sqrt{m^2 + P_\text{T}^2}, \tag{3.1}$$

$$E = m_\text{T} \times \frac{e^Y + e^{-Y}}{2}, \tag{3.2}$$

$$P_x = P_\text{T}\cos(\theta), \tag{3.3}$$

$$P_y = P_\text{T}\sin(\theta), \tag{3.4}$$

$$P_z = m_\text{T} \times \frac{e^Y - e^{-Y}}{2}. \tag{3.5}$$

Before the simulation proceeds further, a pair of simple tests, that are performed to check the validity of the simulation, are primed. We note that these test do

not involve heavy-flavour decay. To be precise, the tests were only necessary until the script was complete and explicitly checking the results after every run is not necessary. However, they were not removed from the script as their existence serves as proof of the validity of the simulation. These tests are done by comparing the results with our input data and checking that they agree with one another. The tests are described in detail in section 3.3.

Having saved the necessary variables in order to later complete the tests, the simulation proceeds to the study of the decay processes. The decay is modelled by inputting the decaying particle to the event record and by using PYTHIA to handle the decay. To be precise, we use the PDG particle code, the particle's mass and the four-momentum defined earlier. Then, once PYTHIA has completed the decay process, we study the results. We wish to compare our results to the ones presented in Ref. [5] and thus we calculate the differential cross section $\frac{1}{2\pi P_T} \frac{d\sigma}{dP_T}$ using the transverse momentum of the hadron and the corresponding cross section. Then, we again save the P_T of the hadron into two temporary histograms, one without weights and one weighted by the differential cross section.

In this work we are particularly interested in the decay particles of heavy-flavour hadrons, in this case only electrons and positrons. They are found by checking the entire event record for their particle codes. In order to make our results comparable to the ones presented in Ref. [5], we only take into account the electrons and positrons whose pseudorapidities are within the interval $-0.35 \leq \eta \leq 0.35$. If a suitable decay particle is found, we calculate the double differential cross section $\frac{1}{2\pi p_T} \frac{d^2\sigma}{dp_T dy}$ using the electron's transverse momentum and the production cross section of the hadron. The electron's p_T is then saved to two temporary histograms one without weights and one weighted by the double differential cross section.

We also wish to combine the results for B- and C-hadron decay electrons/positrons in order to study inclusive heavy-flavour decay. Thus we must, in the case of B-hadron decay, take into account the fact that the decaying particle could decay into a D-meson which would then decay into an electron or a positron. If left unaddressed, this would lead to double counts when the results are combined. Therefore, we take another pair of temporary histograms into which we only save the p_T of the decay particles that do not originate from D-mesons.

3.3   Testing

The main idea of the tests is to check that the sampled events, that have been binned in finite histograms and correctly normalized, correspond to the input data. The value of P_T or rapidity is then saved to two temporary histograms, one without weights and one weighted by the corresponding cross section. Two histograms are used because it is a simple way to obtain both the number of events in a given bin and the sum of the cross sections of said events which are both needed in the normalization described in section 3.4. This procedure is also used when obtaining the actual results of the simulation.

This process continues throughout the event generation and once all the results have been obtained we will need to normalize them. The idea is to use two separate histograms as an easy method of summing the cross sections we used as weights bin by bin and similarly calculating the amount of events in each transverse momentum, or rapidity, bin. Thus, we can calculate the average of the double differential cross sections in each bin as

$$\frac{\mathrm{d}^2\sigma}{\mathrm{d}P_\mathrm{T}\mathrm{d}Y} = \frac{1}{N_j} \times \sum_{i=1}^{N_j} \left(\frac{\mathrm{d}^2\sigma}{\mathrm{d}P_\mathrm{T}\mathrm{d}Y} \right)_i, \tag{3.6}$$

where N_j is the amount of events within the bin and the summation goes over all of said events. This average is then saved into the final histogram, with bins identical to the temporary histograms, into the correct transverse momentum, or rapidity, bin. Finally we check if the average of the double differential cross section in each bin agrees with the input data, that was scaled to account for all possible B- or C-hadrons, as we would expect.

In addition to these results, we will include a numerical prediction for the double differential cross section, $\frac{\mathrm{d}^2\sigma}{\mathrm{d}P_\mathrm{T}\mathrm{d}Y}$. This prediction is obtained by taking a predetermined value of P_T, or rapidity, as a known value and taking a very large amount of rapidity, or P_T, points with a set distance between them so that the entire rapidity, or P_T, range is covered. These known values were chosen to be $P_\mathrm{T} = 2.00$ GeV and $Y = 0.00$ for B-hadrons and $P_\mathrm{T} = 1.00$ GeV and $Y = 0.00$ for C-hadrons. Finally, the cross section is interpolated at all points and the resulting prediction is plotted alongside the scaled input data and the numerical results.

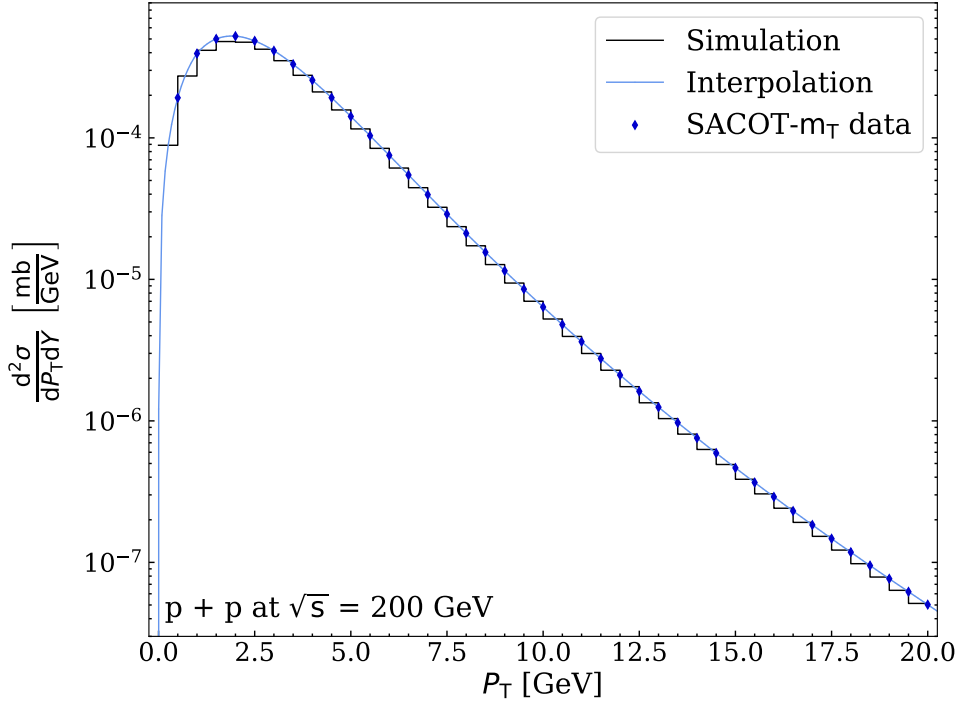The resulting plots are shown in Figures 4 and 5. Figure 4 presents the double

Figure 4. Double differential cross section as a function of transverse momentum at $Y = 0.00$, simulation with $Y \in [-0.50, 0.50]$, for B-hadron production.
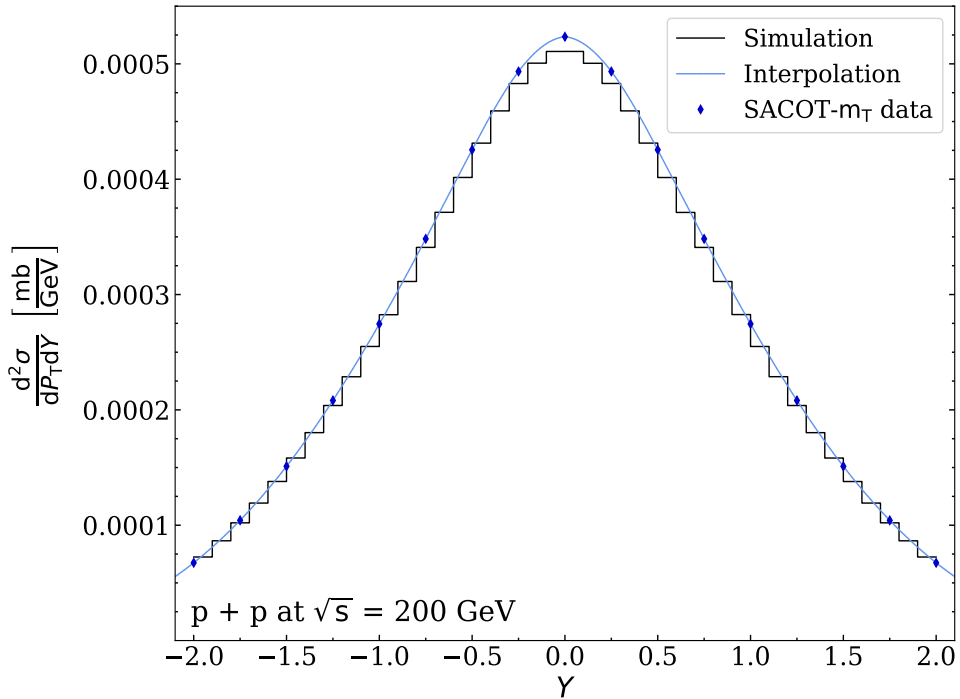

Figure 5. Double differential cross section as a function of rapidity at $P_T = 2.00$ GeV, simulation with $P_T \in [1.50 \text{ GeV}, 2.50 \text{ GeV}]$, for B-hadron production.

differential cross section $\frac{\mathrm{d}^2\sigma}{\mathrm{d}P_\mathrm{T}\mathrm{d}Y}$ at $Y = 0$ as a function of P_T in B-hadron production using the following choice of scales $\mu_\mathrm{fact} = 1.0$, $\mu_\mathrm{ren} = 1.0$, $\mu_\mathrm{frag} = 1.0$. We observe that the results of the simulation match both the prediction and the input data well. However, we notice that the results of the simulation are systematically smaller than the predicted results or the input data. This is to be expected as both the prediction and the input data were obtained using $Y = 0$ as a known value whereas the simulation takes into account the events within a small rapidity interval, $-0.50 \leq Y \leq 0.50$. This difference explains the deviations since the largest cross sections are obtained at $Y = 0$. We also note that, since the prediction matches the input data perfectly, as one would assume, we can conclude that the interpolation is working as expected.

Figure 5 on the other hand presents the double differential cross section $\frac{\mathrm{d}^2\sigma}{\mathrm{d}P_\mathrm{T}\mathrm{d}Y}$ at $P_\mathrm{T} = 2.00$ as a function of Y in B-hadron production using the following choice of scales $\mu_\mathrm{fact} = 1.0$, $\mu_\mathrm{ren} = 1.0$, $\mu_\mathrm{frag} = 1.0$. We again observe that the results of the simulation match the prediction and the scaled input data well and that the prediction matches the input data perfectly, which proves that the interpolation is not flawed. In particular, this is supported by the fact that we observe no deviations while interpolating the transverse momenta with a given rapidity or while interpolating the rapidities with a given transverse momentum. Furthermore, we observe similar small deviations between the numerical results and the data as we did in Figure 4, namely that the simulated results are systematically smaller than the predicted results and the input data. However, we again expect such deviations as the data and the prediction are taken for a precise transverse momentum, in this case $P_\mathrm{T} = 2.00$ GeV, while the numerical results are obtained using a small P_T interval, namely 1.50 GeV $\leq P_\mathrm{T} \leq 2.50$ GeV. This is due to the fact that the largest cross sections for B-hadrons are obtained at approximately $P_\mathrm{T} = 2.00$, as seen in Figure 4.

3.4   Normalization

Once the event generation has been completed and all results have been saved into temporary histograms, we can begin to normalize the results. The normalization follows the logic of the general case of Monte Carlo integration, where each results has its individual weight w_j. Furthermore, since the bins we have used have differing bin widths, we must again perform the normalization in each bin separately. We will denote an arbitrary bin, whose widths are $(\Delta P_\mathrm{T})_i$ and $(\Delta Y)_i$, or $(\Delta y_\mathrm{T})_i$ and $(\Delta y)_i$ if we are dealing with decay products, as B_i. Now, the cross section in each bin is given by

$$\frac{\mathrm{d}^2\sigma}{\mathrm{d}P_\mathrm{T}\mathrm{d}Y} = \frac{1}{(\Delta P_\mathrm{T})_i\,(\Delta Y)_i}\frac{\sigma_\mathrm{int}}{w_\mathrm{tot}} \times \left(\sum_{j\in B_i} w_j\right), \tag{3.7}$$

where σ_int is the integrated cross section, w_tot is the sum of all weights and the sum at the end goes over all results in the bin.

We also know that the integrated cross section in Eq. (3.7) is defined as

$$\sigma_\mathrm{int} = \sum_{j=1}^{N}\left(\frac{\mathrm{d}^2\sigma}{\mathrm{d}P_\mathrm{T}\mathrm{d}Y}\right)_j \times \frac{\Delta P_\mathrm{T}\Delta Y}{N}, \tag{3.8}$$

where N is the total amount of events, $\left(\frac{\mathrm{d}^2\sigma}{\mathrm{d}P_\mathrm{T}\mathrm{d}Y}\right)_j$ is the production cross section of an individual hadron and ΔP_T and ΔY are the widths of the entire ranges of transverse momentum and rapidity. In this work the study was performed within the intervals $P_\mathrm{T} \in [0.00\text{ GeV}, 20.00\text{ GeV}]$ and $Y \in [-2.00, 2.00]$ and therefore we have $\Delta P_\mathrm{T} = 20.00$ GeV and $\Delta Y = 4.00$.

We now recall that we have, in this work, used the particles's cross sections as weights, i.e. $w_j = \left(\frac{\mathrm{d}^2\sigma}{\mathrm{d}P_\mathrm{T}\mathrm{d}Y}\right)_j$. Therefore the sum of the cross sections of all events in Eq. (3.8) is merely the sum of all weights, $w_\mathrm{tot} = \sum_j \left(\frac{\mathrm{d}^2\sigma}{\mathrm{d}P_\mathrm{T}\mathrm{d}Y}\right)_j$, from Eq. (3.7). Therefore, the equation for the integrated cross section simplifies to

$$\sigma_\mathrm{int} = w_\mathrm{tot}\frac{\Delta P_\mathrm{T}\Delta Y}{N}. \tag{3.9}$$

Inserting this form of the integrated cross section into equation (3.7), we obtain

$$\frac{\mathrm{d}^2\sigma}{\mathrm{d}P_\mathrm{T}\mathrm{d}Y} = \frac{1}{(\Delta P_\mathrm{T})_i\,(\Delta Y)_i}\frac{\Delta P_\mathrm{T}\Delta Y}{N} \times \sum_{j\in B_i}\left(\frac{\mathrm{d}^2\sigma}{\mathrm{d}P_T\mathrm{d}Y}\right)_j, \tag{3.10}$$

which is the general form of the cross section we have used.

Now we can easily obtain the exact forms of normalization we have used. While studying the decaying hadrons themselves, we were only interested in the differential cross section $\frac{1}{2\pi P_T}\frac{\mathrm{d}\sigma}{\mathrm{d}P_T}$. The correct normalization is essentially the same as given in Eq. (3.10) but the widths of the rapidity bins are not included. We also note that in this case we must include the factor $\frac{1}{2\pi P_T}$ in the double differential cross sections and therefore the weights. Thus, we have $w_{\mathrm{tot}} = \sum_j \left(\frac{1}{2\pi P_T}\frac{\mathrm{d}^2\sigma}{\mathrm{d}P_T\mathrm{d}Y} \right)_j$. However, this does not otherwise affect the equations. The correctly normalized cross section is therefore

$$\frac{1}{2\pi P_T}\frac{\mathrm{d}\sigma}{\mathrm{d}P_T} = \frac{1}{(\Delta P_T)_i}\frac{\Delta P_T \Delta Y}{N} \times \sum_{j\in B_i}\left(\frac{1}{2\pi P_T}\frac{\mathrm{d}^2\sigma}{\mathrm{d}P_T\mathrm{d}Y} \right)_j . \qquad (3.11)$$

The normalization used for the cross sections of the decay electrons, $\frac{1}{2\pi p_T}\frac{\mathrm{d}^2\sigma}{\mathrm{d}p_T\mathrm{d}y}$, was obtained in a similar manner. However, this time the procedure was more straightforward as we were interested in the double differential cross sections. We only needed to include a factor of $\frac{1}{2}$ to make our results comparable to the experimental data that was averaged as $\sigma = \frac{1}{2}\left(\sigma^{e^-} + \sigma^{e^+} \right)$. The correctly normalized cross section is thus given by

$$\frac{1}{2\pi p_T}\frac{\mathrm{d}^2\sigma}{\mathrm{d}p_T\mathrm{d}y} = \frac{1}{2}\frac{1}{(\Delta p_T)_i (\Delta y)_i}\frac{\Delta P_T \Delta Y}{N} \times \sum_{j\in B_i}\left(\frac{1}{2\pi p_T}\frac{\mathrm{d}^2\sigma}{\mathrm{d}P_T\mathrm{d}Y} \right)_j . \qquad (3.12)$$

3.5 Theoretical uncertainty

The simulation described above naturally contains uncertainty which must be accounted for. In this work, we limit our analysis to the variation of the factorization, renormalization and fragmentation scales that are present in the calculations where the SACOT-m_T scheme is used. We note, that this analysis does not account for all sources of uncertainty, such as PDF and FF uncertainties, and will therefore underestimate the size of the error bands. However, we will assume that scale variation is the predominant source of uncertainty and thus this approach can be deemed sufficient for the purposes of this work. The idea is to vary the scales by a factor of two meaning that we have three possible variations of each scale, namely 0.5, 1.0 and 2.0, leading to a total of 27 possible combinations.

However, not all of these combinations are desirable. This is due to the fact

that the numerical implementation of the SACOT-m_{T} scheme described in Ref. [8] involves logarithms of the form $\log\left(\frac{\mu_{\mathrm{fact}}^2}{\mu_{\mathrm{ren}}^2}\right)$ and $\log\left(\frac{\mu_{\mathrm{ren}}^2}{\mu_{\mathrm{frag}}^2}\right)$. Thus, if we take the factorization and renormalization scales, or the renormalization and fragmentation scales, and vary one of them up and the other down, the absolute values of the logarithms will become artificially large which would lead to very large errors that are, in a sense, artificial. We therefore ignore the 10 combinations that would result in such errors and perform the scale variation with the 17 remaining combinations.

As we mentioned in section 3.1, the simulation described in sections 3.1 – 3.4 is performed separately for the sets of double differential production cross sections obtained with different combinations of the factorization, renormalization and fragmentation scales. Therefore, we obtain an equal number of sets of results. Once the simulation has been performed for all combinations we can use the results to obtain an estimate for the uncertainty due to scale variation. The idea is to study the resulting histograms bin by bin in order to obtain the final results.

More precisely, we take the results obtained using the combination $\mu_{\mathrm{fact}} = 1.0$, $\mu_{\mathrm{ren}} = 1.0$, $\mu_{\mathrm{frag}} = 1.0$ and then compare the results obtained using the other combinations in order to obtain the maximum and minimum values for the cross section and use them as the limits of the error band. We repeat this for each bin. Note that the maximum or minimum values in different bins need not originate from the same variation of the scales. This procedure is used for both the differential production cross sections of the hadrons and the double differential cross sections of the decay electrons and positrons.

This procedure is illustrated in Figures 6 and 7. Figure 6 displays the results obtained for the cross sections of the B-hadron decay events, with all 17 possible combinations of the varied scales and the ratios between each of these results and the main results, i.e. the results obtained using the combination $\mu_{\mathrm{fact}} = 1.0$, $\mu_{\mathrm{ren}} = 1.0$, $\mu_{\mathrm{frag}} = 1.0$. From it we can see that the maximum and minimum values of the cross section are obtained with different combinations of the scales in different regions of the p_{T} interval. Furthermore, we notice that the deviations between the results obtained from different simulations are particularly large in the low-p_{T} region.

Similarly Figure 7 displays the results obtained for the cross sections of the C-hadron decay events, with all possible combinations of the varied scales. We again observe that the maximum and minimum values are obtained with different combinations of the scales in different p_{T} regions. Furthermore, the deviations

between the results obtained from different simulations show a similar behaviour in the low p_T region as observed in Figure 6, namely that they become smaller as p_T increases.
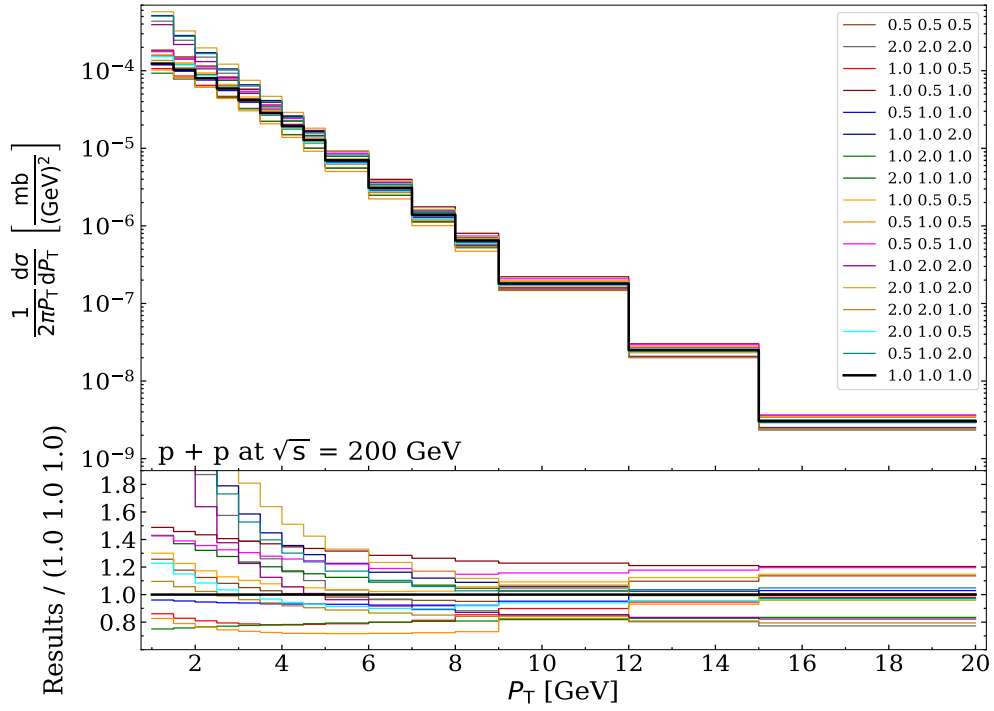
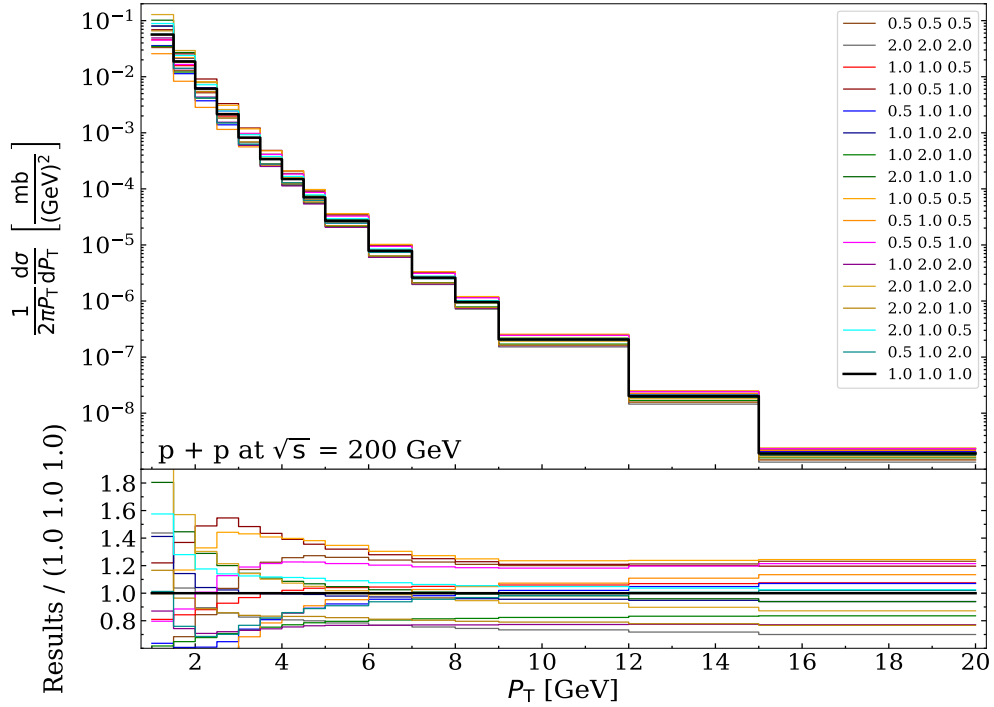**Figure 6.** Differential cross sections for B-hadron production with all scale combinations.

Figure 7. Differential cross sections for C-hadron production with all scale combinations.

4 Results

In order to assess the validity of our numerical approach we will, as mentioned in section 1, compare our results with the experimental results obtained by the PHENIX Collaboration in Ref. [5]. First we will discuss the differential production cross sections of the hadrons themselves. These results were obtained by performing a simulation with 50 million events, where we have, as mentioned in section 3, used the production cross sections obtained with SACOT-m_T as a starting point and simulated the decays of different kinds of B- or C-hadrons in correct proportions.

In Figure 8 we present our numerical results for the differential cross sections of B-hadron production, with the estimated error bands, and compare them with the data from Ref. [5]. In Figure 8, we also plot the ratio between the experimental data and our numerical results. We observe that the numerical results seem to match the experimental data very well as all datapoints are within the error bands. In addition, the errorbands are significantly large in the low-P_T region and reduce in size as P_T increases, which is a direct consequence of the behaviour observed in Figures 6 and 7. As a whole, Figure 8 shows that the SACOT-m_T scheme is in good agreement with experimental data.

The results for C-hadron production, displayed in Figure 9, where we again plot our results alongside the experimental datapoints and also include their ratio, seem somewhat lacking. The numerical results for the differential cross section match the experimental data well in the low-P_T region, but at higher values of P_T significant deviations are observed. However, we must take into account that, as mentioned in section 3.5, we have not taken into account all sources of uncertainty and have thus most likely underestimated the magnitude of the uncertainty in our results. Therefore, as most datapoints only are only slightly beyond the limits of uncertainty we may again conclude that the SACOT-m_T scheme is in agreement with experimental data, but that the agreement seems to suffer at larger values of P_T.
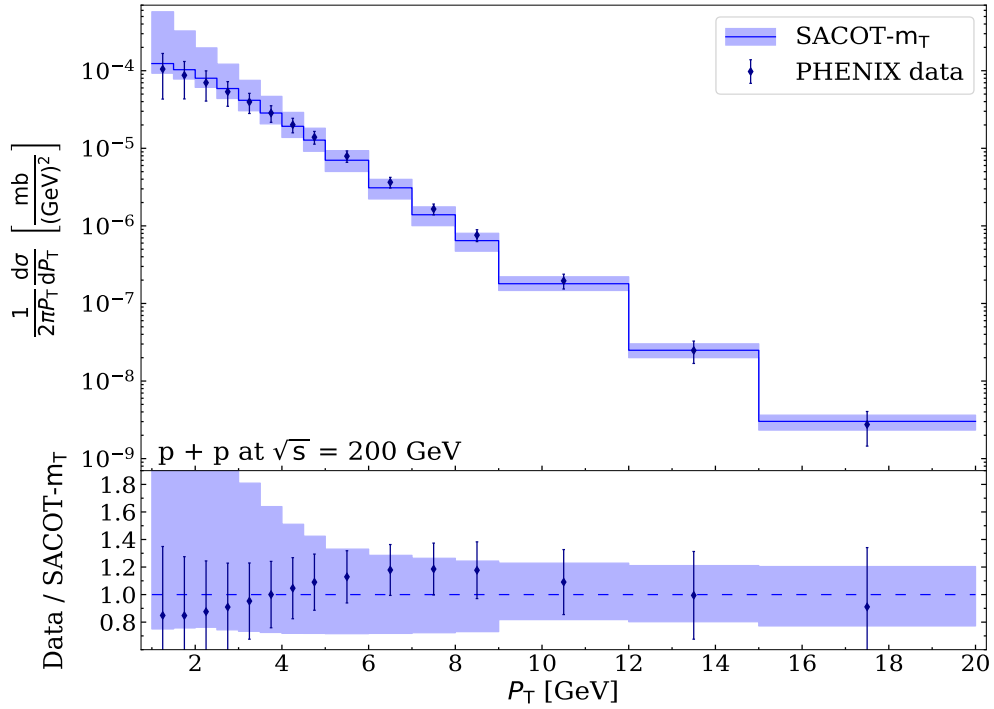
Figure 8. Differential cross sections for B-hadron production alongside experimental datapoints from the PHENIX Collaboration [5].
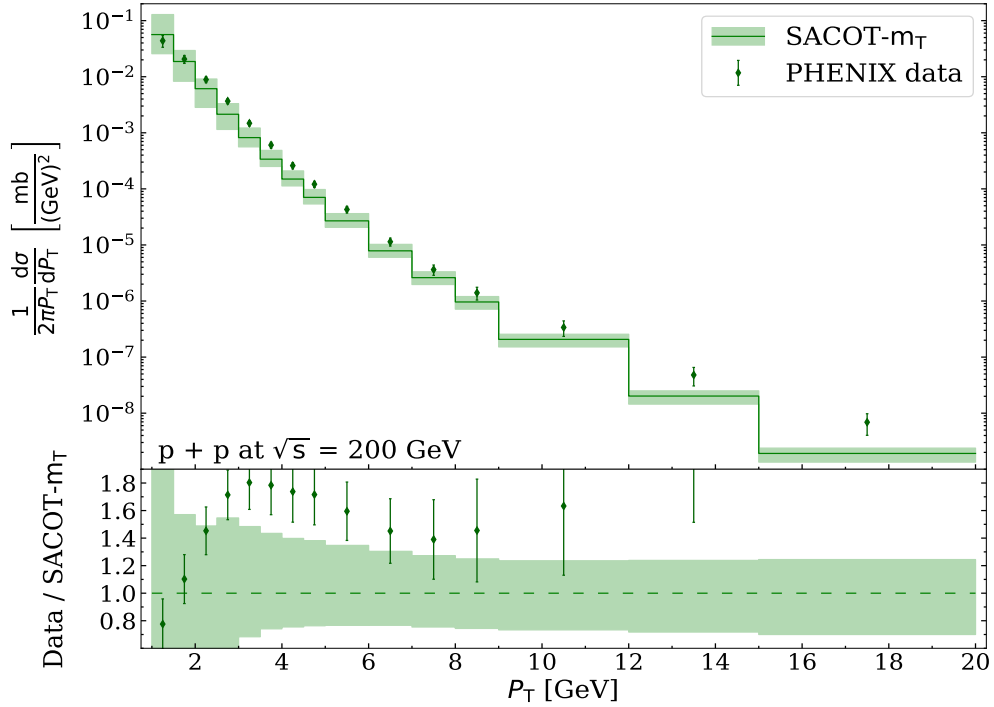

Figure 9. Differential cross sections for C-hadron production alongside experimental datapoints from the PHENIX Collaboration [5].

Now we can address the main results of this work, namely the double differential production cross sections of electrons and positrons in heavy-flavour decay. Here we have, as discussed in section 3.2, taken all events where desired decay particles, namely electrons and positrons, are produced and studied the decay particles individually. Our results are again compared with the experimental results presented in Ref. [5] and the ratio between the experimental data and the numerical results is also included in Figures 10 and 11. Furthermore, we have also compared our results with theoretical FONLL calculations [26].

Figure 10 displays the results for B-hadron decay electrons and positrons. We also note that here we do not filter the decay processes in which an electron or a positron is produced by a decaying D-meson which was produced earlier in the decay process. We observe some small deviation when the transverse momentum is above 4 GeV, but otherwise the numerical and experimental results are in good agreement with one another. However, we also notice that the experimental datapoints are systematically above the numerical results, which implies that the simulation might underestimate the double differential cross sections albeit only slightly.
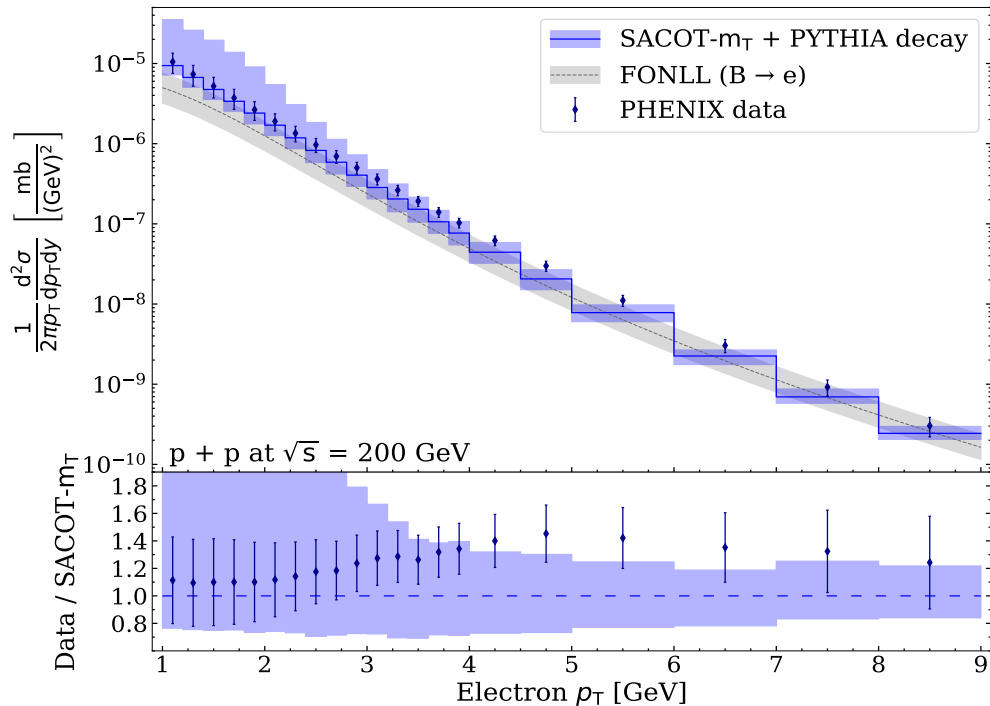

Figure 10. Double differential cross sections for e^+/e^- production, averaged as $(e^+ + e^-)/2$, in B-hadron decay alongside experimental datapoints from the PHENIX Collaboration [5], and a FONLL calculation [26].
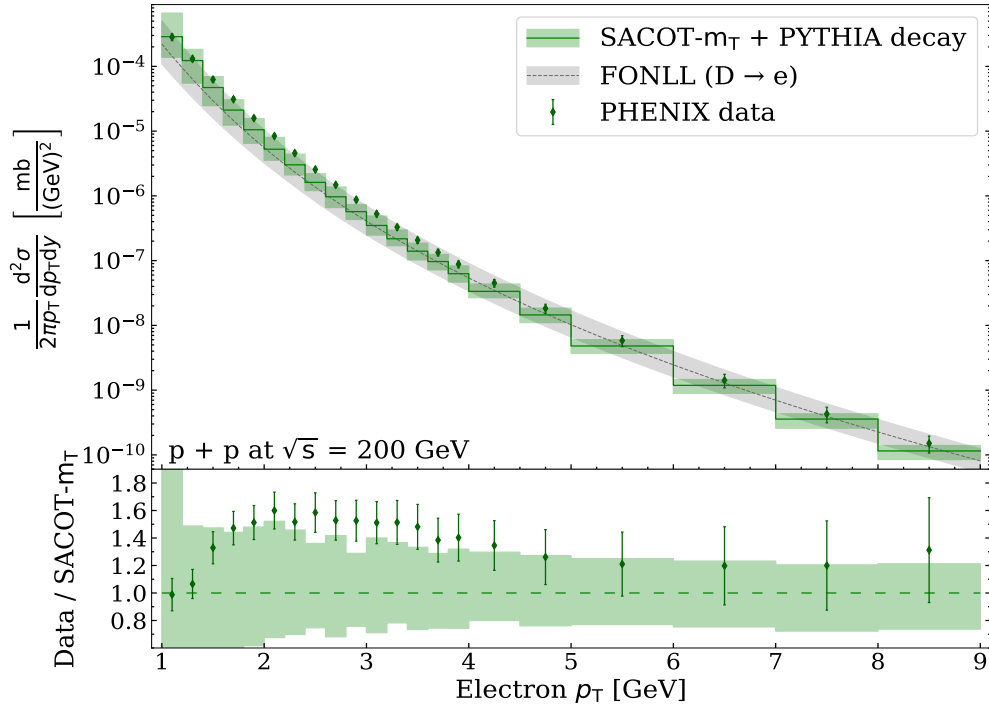
Figure 11. Double differential cross sections for e^+/e^- production, averaged as $(e^+ + e^-)/2$, in C-hadron decay alongside experimental datapoints from the PHENIX Collaboration [5] and a FONLL calculation [26].

Similar behaviour is also observed in Figure 11, where the results for C-hadron decay are presented. We note that only the first datapoint is slightly beneath the numerical result. We again observe that the deviations between theoretical and experimental results in C-hadron decay are slightly larger than in B-hadron decay. However, the deviations observed in Figure 11 are significantly smaller than the ones observed in Figure 9. All in all, we observe a decent correspondence between the numerical and experimental results.

We also observe that the theoretical FONLL calculation are in good agreement with our results. We notice that in both B- and C-hadron decay the correspondence between our numerical results and the FONLL calculation improves as the transverse momentum increases. Moreover, in the low-p_T region we observe that the FONLL calculation gives slightly smaller values for the double differential cross section than our simulation, as can be seen in Figures 10 and 11. This difference is larger in B-hadron decay than in C-hadron decay, albeit only slightly. However, since the limits of uncertainty overlap, we conclude that our results and the FONLL calculations are in agreement with one another.

Based on the observations made from Figures 10 and 11, we can conclude that our simulation produces results that are in agreement with experimental data, albeit it would seem that the simulation slightly underestimates the double differential cross sections in comparison to the experimental results. In B-hadron decay the results are underestimated by 10–40% whereas the results in C-hadron decay the results are underestimated by 0–60%. However, as the most of the datapoints are nonetheless within the uncertainties of the theoretical results or only slightly beyond them, we can still consider our results to be in agreement with the experimental results. Furthermore, based on the results it would seem that the SACOT-m_{T} scheme produces results that are in better agreement with the experimental results than the FONLL calculations are.

We note that the FONLL calculations were done at 200 GeV using the current default parameters with CTEQ6.6 PDFs. For C-hadrons we used D0 as the hadronic final state. The central values were $m_b = 4.75$ GeV, $m_c = 1.5$ GeV and $\mu_R = \mu_F = \mu_0 = \sqrt{m^2 + p_{\mathrm{T}}^2}$. The scales uncertainties were $\frac{\mu_0}{2} < \mu_R$, $\mu_F < 2\mu_0$ with $\frac{1}{2} < \frac{\mu_R}{\mu_F} < 2$, and the mass uncertainties were $m_b = 4.5, 5.0$ GeV and $m_c = 1.3, 1.7$ GeV summed in quadrature to scales uncertainties. The PDF uncertainties were calculated according to the individual PDF set recipe and summed in quadrature to scales and mass uncertainties. Finally, the branching ratios that were used were BR(D $\rightarrow$ l) = 0.103, BR(B $\rightarrow$ l) = 0.1086, BR(B $\rightarrow$ D $\rightarrow$ l) = 0.096, BR(B $\rightarrow$ D) = 0.823, BR(B $\rightarrow$ D*) = 0.173, BR(B $\rightarrow$ J/ψ) = 0.0116 and BR(B $\rightarrow$ $\psi(2S)$) = 0.00307.

In addition to the previous results, we have also considered the decay particles in inclusive heavy-flavour decays. To be precise, we have, as mentioned in section 3.2, combined our results for B- and C-hadron decay electrons/positrons. However, in order to avoid double counts we had to filter out the B-hadron decays in which the decay electrons or positrons originate from a D-meson, as explained in section 3.2. These results are then compared with experimental results from Ref. [27]. In Figure 12, we display these results alongside the results for both B- and C-hadron decay. We observe that our results are in agreement with the experimental results in the low-p_{T} region but at larger p_{T} the difference becomes significant. This behaviour is to be expected as our results were systematically smaller than the experimental results for both B- and C-hadron decay, as discussed above. Because of this we conclude that there is reasonable agreement between our results and the numerical results.
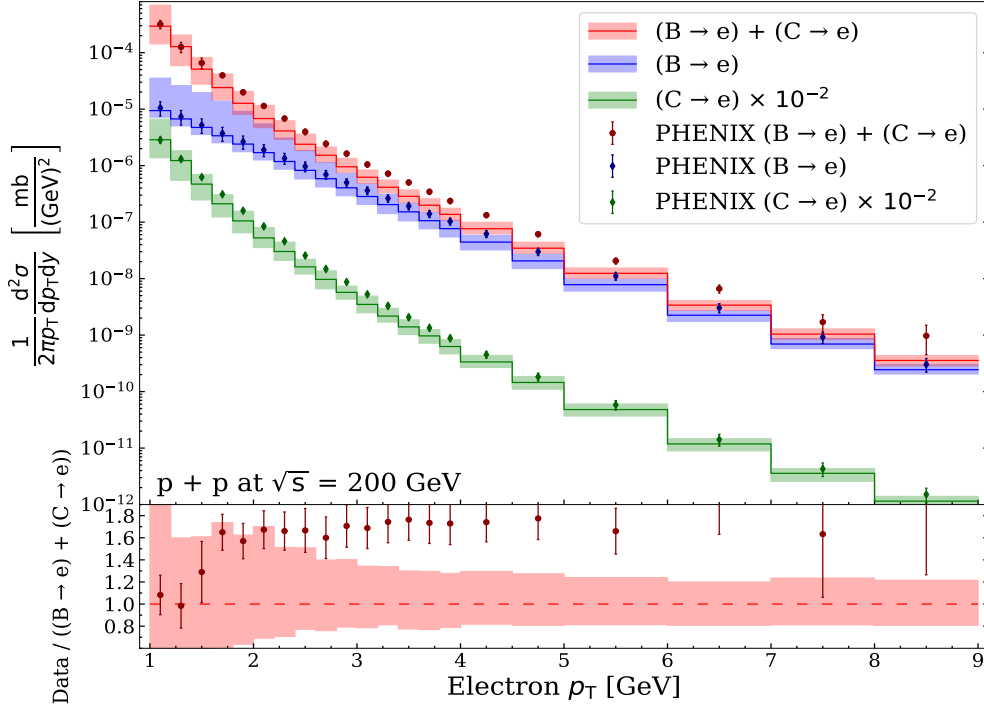
Figure 12. Collected double differential cross sections for e^+/e^- alongside experimental data from the PHENIX Collaboration for $(B \to e)$ and $(C \to e)$ [5] and for $(B \to e) + (C \to e)$ [27].

We were also interested in the fraction of electrons that are formed in B-hadron decay when compared to the inclusive case. Our results alongside experimental data presented in Ref. [5] are displayed in Figure 13. We observe that our results are, for the most part, in very good accordance with the experimental data. However, when compared with the experimental data, our central results seem to overestimate the data by 20–30% when the transverse momentum is around 1.50–2.75 GeV. We notice that this is most likely related to the fact that, as seen from Figures 10 and 11, the amount by which the results for B-hadron decay particles are underestimated is significantly less than the amount by which the results for C-hadron decay particles are underestimated when p_{T} is around 1.50–2.75 GeV. Otherwise, the deviations are much smaller. Therefore we conclude that the correspondence between numerical and experimental results is good which supports our earlier conclusion that the simulation produces results that are in good agreement with experimental data.
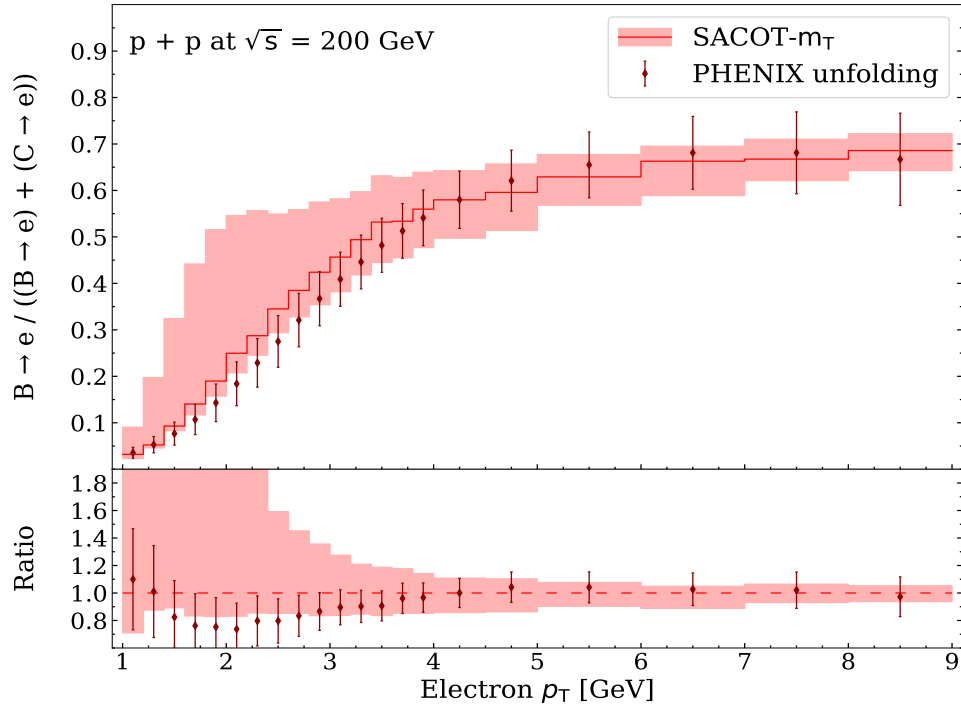
Figure 13. Fraction of bottom electrons plotted alongside experimental data from the PHENIX Collaboration [5].

5 Conclusions

The purpose of this thesis was to study the semileptonic decays of heavy-flavour hadrons and to serve as a test for the validity of the so-called SACOT-m_T scheme. This was done by creating a simulation in which the decays of heavy-flavour hadrons, whose production cross sections were obtained with a numerical implementation of the SACOT-m_T scheme, first introduced in Ref. [8], were modelled with the PYTHIA event generator [9]. The obtained results were then compared with existing theoretical predictions, in this case FONLL calculations [26], and experimental data.

As discussed in section 4, the obtained theoretical results were for the most part in good accordance with the experimental results. This supports the conclusion that the theoretical setup is sufficient to describe experimental results. This conclusion is further supported by the fact that a good correspondence is observed regardless of the fact that the size of the uncertainties is likely somewhat underestimated in our results, as discussed in section 3.5. Furthermore, we observed that the results for e^+/e^- production were also in agreement with FONLL calculations in both B- and C-hadron decay.

Based on these observations we can conclude that the simulation functions without major flaws. Furthermore, this implies that the numerical implementation of the SACOT-m_T scheme must also function without major flaws, as it was used to obtain our input data and therefore serves as the foundation of the study performed in this thesis. These conclusions thus serve as proof of the validity of the use of the SACOT-m_T scheme. Furthermore, the fact that we were able to obtain results that are in agreement with both experimental data and FONLL calculations throughout the entire kinematic range underlines the usefulness of the SACOT-m_T scheme.

Even though the obtained theoretical results match the experimental data, there is still room for improvement. The most obvious manner in which the analysis could be improved would be to modify the estimation of uncertainty to take into account other sources of uncertainty in addition to the variation of scales. This would allow us to asses the validity of our assumption about scale variation being the predominant source of uncertainty and the produced results would be more realistic.

One way to expand the numerical setup would be to modify it to study other decay particles besides electrons and positrons. In fact, the required framework is already present in the simulation, as mentioned in section 3.1. We only limited our study to the decay electrons and positrons because it was deemed sufficient for the purposes of this work. Studying other decay processes, such as B $\rightarrow$ J/Ψ, would also allow us to perform further comparison between numerical and experimental data, which would allow us to further assess the validity of the use of the SACOT-m_{T} scheme.

References

[1]   M. Gell-Mann. "A Schematic Model of Baryons and Mesons". In: *Phys. Lett.* 8 (1964), pp. 214–215. DOI: 10.1016/S0031-9163(64)92001-3.

[2]   G. Zweig. "Fractionally charged particles and SU_6". In: *2nd International School of Physics "Ettore Majorana"*. 1965, pp. 192–234. DOI: 10.1016/B978-1-4832-5648-1.50011-7.

[3]   R. L. Workman et al., (Particle Data Group). "Review of Particle Physics". In: *PTEP* 2022 (2022), p. 083C01. DOI: 10.1093/ptep/ptac097.

[4]   M. Cacciari, M. Greco, and P. Nason. "The P(T) spectrum in heavy flavor hadroproduction". In: *JHEP* 05 (1998), p. 007. DOI: 10.1088/1126-6708/1998/05/007. arXiv: hep-ph/9803400.

[5]   C. Aidala et al., (PHENIX). "Measurement of charm and bottom production from semileptonic hadron decays in $p + p$ collisions at $\sqrt{s_{NN}} = 200$ GeV". In: *Phys. Rev. D* 99.9 (2019), p. 092003. DOI: 10.1103/PhysRevD.99.092003. arXiv: 1901.08405 [hep-ex].

[6]   A. Andronic et al. "Heavy-flavour and quarkonium production in the LHC era: from proton–proton to heavy-ion collisions". In: *Eur. Phys. J. C* 76.3 (2016), p. 107. DOI: 10.1140/epjc/s10052-015-3819-5. arXiv: 1506.03981 [nucl-ex].

[7]   S. H. Sebastian, ALICE. "Future ALICE upgrades for Run 4 and Beyond". In: *29th International Conference on Ultra-relativistic Nucleus-Nucleus Collisions*. Nov. 2022. arXiv: 2211.04802 [nucl-ex].

[8]   I. Helenius and H. Paukkunen. "Revisiting the D-meson hadroproduction in general-mass variable flavour number scheme". In: *JHEP* 05 (2018), p. 196. DOI: 10.1007/JHEP05(2018)196. arXiv: 1804.03557 [hep-ph].

[9]   C. Bierlich et al. "A comprehensive guide to the physics and usage of PYTHIA 8.3". In: (Mar. 2022). DOI: 10.21468/SciPostPhysCodeb.8. arXiv: 2203.11601 [hep-ph].

[10] D. E. Soper. "Parton distribution functions". In: *Nucl. Phys. B Proc. Suppl.* 53 (1997). Ed. by C. Bernard et al., pp. 69–80. DOI: `10.1016/S0920-5632(96)00600-7`. arXiv: `hep-lat/9609018`.

[11] R. D. Ball et al. "Parton distributions with LHC data". In: *Nucl. Phys. B* 867 (2013), pp. 244–289. DOI: `10.1016/j.nuclphysb.2012.10.003`. arXiv: `1207.1303 [hep-ph]`.

[12] A. Metz and A. Vossen. "Parton Fragmentation Functions". In: *Prog. Part. Nucl. Phys.* 91 (2016), pp. 136–202. DOI: `10.1016/j.ppnp.2016.08.003`. arXiv: `1607.02521 [hep-ex]`.

[13] P. Nason, S. Dawson, and R. K. Ellis. "The Total Cross-Section for the Production of Heavy Quarks in Hadronic Collisions". In: *Nucl. Phys. B* 303 (1988), pp. 607–633. DOI: `10.1016/0550-3213(88)90422-1`.

[14] P. Nason, S. Dawson, and R. K. Ellis. "The One Particle Inclusive Differential Cross-Section for Heavy Quark Production in Hadronic Collisions". In: *Nucl. Phys. B* 327 (1989). [Erratum: Nucl.Phys.B 335, 260–260 (1990)], pp. 49–92. DOI: `10.1016/0550-3213(89)90286-1`.

[15] F. Aversa et al. "QCD Corrections to Parton-Parton Scattering Processes". In: *Nucl. Phys. B* 327 (1989), p. 105. DOI: `10.1016/0550-3213(89)90288-5`.

[16] V. N. Gribov and L. N. Lipatov. "Deep inelastic e p scattering in perturbation theory". In: *Sov. J. Nucl. Phys.* 15 (1972), pp. 438–450.

[17] V. N. Gribov and L. N. Lipatov. "e+ e- pair annihilation and deep inelastic e p scattering in perturbation theory". In: *Sov. J. Nucl. Phys.* 15 (1972), pp. 675–684.

[18] G. Altarelli and G. Parisi. "Asymptotic Freedom in Parton Language". In: *Nucl. Phys. B* 126 (1977), pp. 298–318. DOI: `10.1016/0550-3213(77)90384-4`.

[19] Y. L. Dokshitzer. "Calculation of the Structure Functions for Deep Inelastic Scattering and e+ e- Annihilation by Perturbation Theory in Quantum Chromodynamics." In: *Sov. Phys. JETP* 46 (1977), pp. 641–653.

[20] B. A. Kniehl et al. "Inclusive B-Meson Production at the LHC in the GM-VFN Scheme". In: *Phys. Rev. D* 84 (2011), p. 094026. DOI: `10.1103/PhysRevD.84.094026`. arXiv: `1109.2472 [hep-ph]`.

[21] R. V. Gavai et al. "Heavy quark production in *pp* collisions". In: *Int. J. Mod. Phys. A* 10 (1995), pp. 2999–3042. DOI: `10.1142/S0217751X95001431`. arXiv: `hep-ph/9411438`.

[22] M. Cacciari and M. Greco. "Large p_T hadroproduction of heavy quarks". In: *Nucl. Phys. B* 421 (1994), pp. 530–544. DOI: `10.1016/0550-3213(94)90515-0`. arXiv: `hep-ph/9311260`.

[23] I. Helenius and H. Paukkunen. "B-meson hadroproduction in the SACOT-m_T scheme". In: (Mar. 2023). arXiv: `2303.17864 [hep-ph]`.

[24] F. Halzen and A. D. Martin. *Quarks and Leptons: An Introductory Course in Modern Particle Physics*. New York: Wiley, 1984.

[25] E. Lohrmann. "A Summary of Charm Hadron Production Fractions". In: (Dec. 2011). arXiv: `1112.3757 [hep-ex]`.

[26] M. Cacciari, P. Nason, and R. Vogt. "QCD predictions for charm and bottom production at RHIC". In: *Phys. Rev. Lett.* 95 (2005), p. 122001. DOI: `10.1103/PhysRevLett.95.122001`. arXiv: `hep-ph/0502203`.

[27] A. Adare et al., (PHENIX). "Heavy Quark Production in $p + p$ and Energy Loss and Flow of Heavy Quarks in Au+Au Collisions at $\sqrt{s_{NN}} = 200$ GeV". In: *Phys. Rev. C* 84 (2011), p. 044905. DOI: `10.1103/PhysRevC.84.044905`. arXiv: `1005.1627 [nucl-ex]`.

A   Simulation code and datapoints

The simulation code alongside other relevant codes and the datapoints can be found at:

https://gitlab.jyu.fi/amtolvau/semileptonic-decays-of-heavy-flavour-hadrons